Forschungszentrum Karlsruhe
Technik und Umwelt

Wissenschaftliche Berichte
FZKA 5717

MHD Flow Structure in Bends Perpendicular or Partly Parallel to the Magnetic Field

J. Reimann, I. Bucenieks, L. Bühler, S. Dementjev, A. Flerov, S. Molokov, I. Platnieks

Institut für Angewandte Thermo- und Fluiddynamik
Projekt Kernfusion

März 1996

FORSCHUNGSZENTRUM KARLSRUHE
Technik und Umwelt
Wissenschaftliche Berichte
FZKA 5717

MHD FLOW STRUCTURE IN BENDS PERPENDICULAR OR PARTLY PARALLEL TO THE MAGNETIC FIELD

J. Reimann, I. Bucenieks[a)], L. Bühler, S. Dementjev[a)], A. Flerov[a)], S. Molokov[b)], I. Platnieks[a)]

Institut für Angewandte Thermo- und Fluiddynamik
Projekt Kernfusion
Association Forschungszentrum Karlsruhe / EURATOM
a) Latvian Academy of Sciences, IP, Salaspils 1, LV-2169, Latvia
b) University of Oxford, Department of Engineering Science,
19, Parks Road, Oxford OX1 3PJ, Great Britain

Forschungszentrum Karlsruhe GmbH, Karlsruhe
1996

Als Manuskript gedruckt

Forschungszentrum Karlsruhe GmbH
Postfach 3640, 76021 Karlsruhe

ISSN 0947-8620

MHD FLOW STRUCTURE IN BENDS PERPENDICULAR OR PARTLY PARALLEL TO THE MAGNETIC FIELD

ABSTRACT

This report describes results on the flow structure (distributions of mean velocities, velocity fluctuations and signal spectra) in magnetohydrodynamic (MHD) flow in 90° bends. These bends were either perpendicular or partly parallel to the magnetic field. The experiments were carried out in mercury flow with Hartmann numbers and Interaction parameters of $0 \leq Ha \leq 550$ and $0 \leq N \leq 150$. Ducts with both electrical conducting and nonconducting walls were investigated. Velocity distributions were measured in different duct cross sections using traversable hot wire probes or different types of electric potential probes. The velocity distributions were also evaluated by theoretical analyses valid for inertialess laminarized flow.

For both types of bend orientations significant differences to the theoretical predictions occur in the bend region due to the local influence of inertial forces. Strong flow instabilities with axis parallel to the magnetic field are observed in both cases which can persist for a quite long distance in the downstream duct, depending on the MHD parameters. Different generation mechanisms for these vortices exist: For the bend perpendicular to B, inertia effects near the inner corner play a dominant role and, for electrically conducting duct walls, the M shaped velocity profile in the downstream duct. For bends with the downstream duct parallel to B, inertial forces in combination with the enforced M shaping of the velocity distribution in the inlet duct are of prime importance.

In duct flows with heat transfer, these MHD flow instabilities are expected to prevent the formation of hot spots in the bend regions and might be still effective for an improved heat removal in a significant part of the downstream duct.

MHD STRÖMUNGSSTRUKTUR IN KRÜMMERN SENKRECHT ODER TEILWEISE PARALLEL ZUM MAGNETISCHEN FELD

ZUSAMMENFASSUNG

Dieser Bericht beschreibt Ergebnisse über die Strömungsstruktur (Verteilungen der zeitlich gemittelten Geschwindigkeiten, der Geschwindigkeitsverteilungen und Signalspektren) von magnetohydrodynamischer (MHD) Strömung in 90° Krümmern. Diese Krümmer waren entweder senkrecht oder teilweise parallel zum magnetischen Feld angeordnet. Die Experimente fanden in Quecksilber-Strömung statt bei Hartmann-Zahlen und Interaktions-Parametern von $0 \leq Ha \leq 550$ und $0 \leq N \leq 150$. Es wurden Kanäle mit sowohl elektrisch leitenden als auch nichtleitenden Wänden untersucht. Die Geschwindigkeitsverteilungen wurden mit Hitzdrahtsonden oder verschiedenen Typen von elektrischen Potentialsonden in verschiedenen Kanalquerschnitten gemessen. Die Geschwindigkeitsverteilungen wurden weiterhin durch theoretische Analysen bestimmt, gültig für trägheitsfreie laminare Strömung.

In beiden Kanaltypen treten wesentliche Unterschiede zu den theoretischen Ergebnissen im Bereich des Krümmers auf, hervorgerufen durch den lokalen

Einfluß von Trägheitskräften. Es werden ausgeprägte Strömungsinstabilitäten mit Achsen parallel zum Magnetfeld beobachtet, die, abhängig von MHD Parametern, über eine recht lange Lauflänge im Kanal stromab des Krümmers bestehen können. Die Erzeugungsmechanismen für diese Wirbel sind unterschiedlich: Für senkrecht zum Magnetfeld angeordnete Krümmer spielen Trägheitskräfte nahe der inneren Ecke eine dominierende Rolle und für elektrisch leitfähige Kanalwände das M-förmige Geschwindigkeitsprofil im strom-abgelegenen Kanal. Für Krümmer, bei denen dieser Kanal parallel zu B angeordnet ist, sind Trägheitskräfte in Verbindung mit einem verstärkten M-förmigen Geschwindigkeitsprofil im Eintrittskanal von wesentlicher Bedeutung. Es wird erwartet, daß die MHD-Turbulenz die Bildung von Heißstellen im Krümmerbereich verhindert und auch in einem beträchtlichen Bereich stromab sich noch günstig auf den Wärmeübergang auswirkt.

CONTENTS

1. INTRODUCTION

The investigations described in this report are related to the design of liquid metal cooled blankets for fusion reactors. An important concern for these blankets are magnetohydrodynamic (MHD) effects and their influence on heat and mass transfer processes. MHD effects might overwhelm viscous and inertia effects, resulting in suppression of usual turbulence and radically alter flow structures. (In this report the term flow structure comprises the distribution of mean and fluctuating velocity components and spectra of these fluctuations).

In the past, experimental investigations for fusion reactor blankets concentrated on the determination of pressure drop in various flow components mostly perpendicular to the magnetic field. Flow profiles, however, were in general determined only theoretically based on assumptions valid for laminar, inertialess MHD flow /1-4/. These assumptions appeared to be reasonable because theoretical results for pressure drop often agree fairly well with experimental results for a wide range of MHD parameters. However, it has been known for many years that strong flow instabilities or a significant anisotropic turbulence might exist /5-8/ which does not cause a noticeable pressure drop. The exploitation of this "MHD turbulence" could significantly improve the heat transfer characteristics and thus simplify blanket designs /9/.

This report describes investigations on the structure of MHD flow in different types of bends. Of particular interest is if these bends can act as promotors for flow instabilities. In MHD flow the orientation of the bend in respect to the magnetic field direction is a very important parameter. Essentially, two different cases are of interest for technical applications: bends with ducts perpendicular to the magnetic field B or bends where one duct is perpendicular to B and the other is parallel to B.

An example for the latter case is shown in Fig. 1a). In this blanket concept /1/ the "radial" ducts (perpendicular to B) by 90° bends with the "toroidal" ducts (parallel to B) which must remove from the "first wall"(FW) heat flux from the plasma.

Bends with one duct parallel to B are of technical interest because the pressure drop in a duct parallel to B is negligible compared to that one in a duct perpendicular to B. However, the change of the flow direction in respect to B

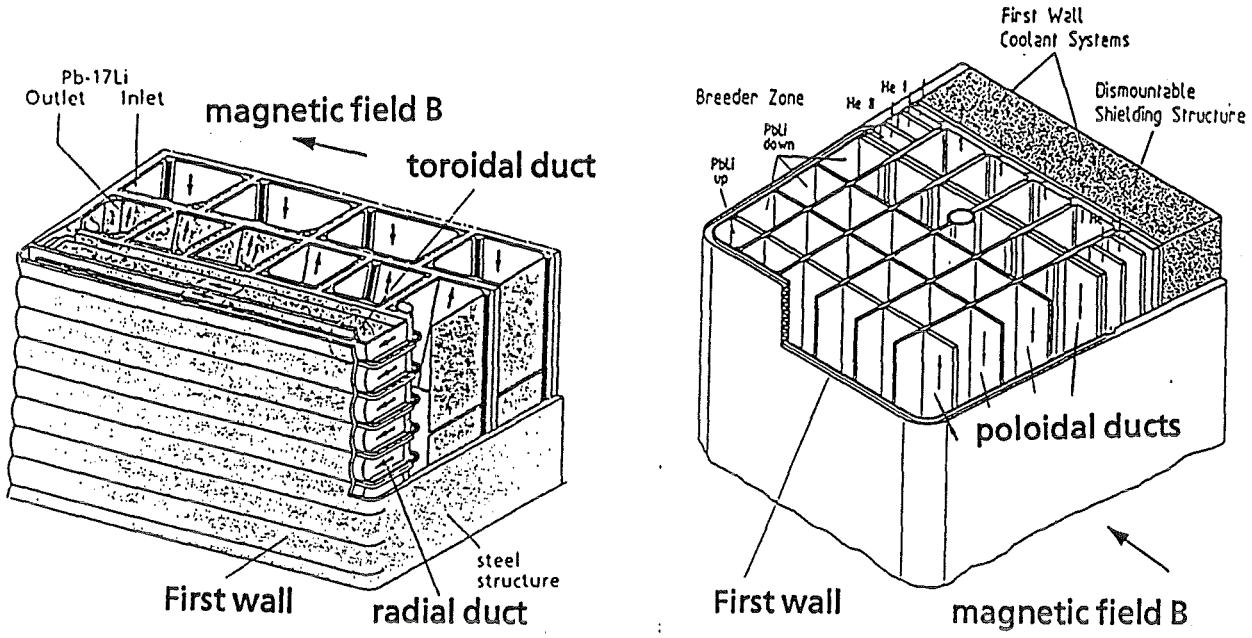

a) b)

Fig. 1.1 Liquid metal-cooled blankets developed in FZK: a) Self-cooled Pb-17Li blanket based on radial-toroidal flow concept /1/; b) Dual-Coolant Concept mainly based on poloidal flow /2/.

causes three-dimensional (3d) electric currents in the bend region which result in an additional bend pressure drop which is for inertialess MHD flow of the order of the pressure drop over a characteristic length in a two-dimensional (2d) duct flow. For inertial flow this additional pressure drop increases with increasing velocity and decreasing magnetic field strength, details for different duct geometries are given in /10, 11/.

For the U-bend geometry the two 90° bends are electrically connected by a global current circuit and the pressure drop is increased compared to that one for a single 90° bend. The dependencies of this additional pressure drop on the duct parameters and MHD parameters are given in /10-12/. Therefore, pressure drop can presently be predicted with an accuracy sufficient for technical applications.

The change of the flow direction with respect to magnetic field direction leads to very different flow patterns in the upstream and downstream duct. These distributions were up to now only predicted theoretically for laminar inertialess flow. (A certain experimental verification was obtained by a good agreement between numerous measured and predicted electric wall potentials /10, 11/). Due to the importance of the flow distribution for heat transfer the present

investigations were performed. The flow structure at the entrance of the downstream duct is of prime importance because hot spots might occur.

Bends with ducts perpendicular to B are part of many blanket designs. In the Dual Coolant Blanket /2/ this flow geometry exists at the blanket bottom (Fig. 1b) where the downward flow in poloidal direction is deflected into the radial direction and then again in a 90° bend into the upward poloidal direction.

The flow in this kind of bends is characterized by two-dimensional (2d) current distributions which do not result in remarkable additional pressure drops as predicted theoretically for inertialess flor /4/ and verified experimentally for a wide range of MHD parameters /13/. Another characteristic features are short flow lengths upstream and downstream of the bend where fully developed flow is restored. Therefore, the mutual influence of the 90° bends in a U-bend becomes negligible for quite small lengths of the duct inbetween. Again direct measurements of the flow structure did not exist prior to the present investigations.

In this report detailed results of investigations are presented on the flow structure in bends with the two different orientations to the magnetic field B, as outlined above. Some singular results published before, see /14, 15/. The following designations are used: "bpeB" stands for bend perpendicular to B and "bpaB" holds for bend partly parallel to B.

2. EXPERIMENTAL

2.1 Test Loop and Test Sections

The experiments were performed in the MHD laboratory of the Institute of Physics of the Latvian Academy of Sciences. Mercury (Hg) was used as liquid metal. A magnet with circular pole shoes was used with a homogeneous magnetic field for a diameter of 400 mm. An electromagnetic (EM) pump circulated the liquid metal in the loop. Flow rates were measured with an EM flow meter which could be calibrated by means of a venturi nozzle. The Hg temperature was kept constant by means of a water-cooler.

Fig. 2.1 shows schematically the test section (which was used in both types of experiments) and its arrangement for the bpaB experiments. The test section consists of two 90° bends connected by the duct parallel to B. This U-bend geometry is representative for the blanket shown in Fig. 1a. Therefore, again the designations radial and toroidal, are used for the bpaB experiments, as defined before.

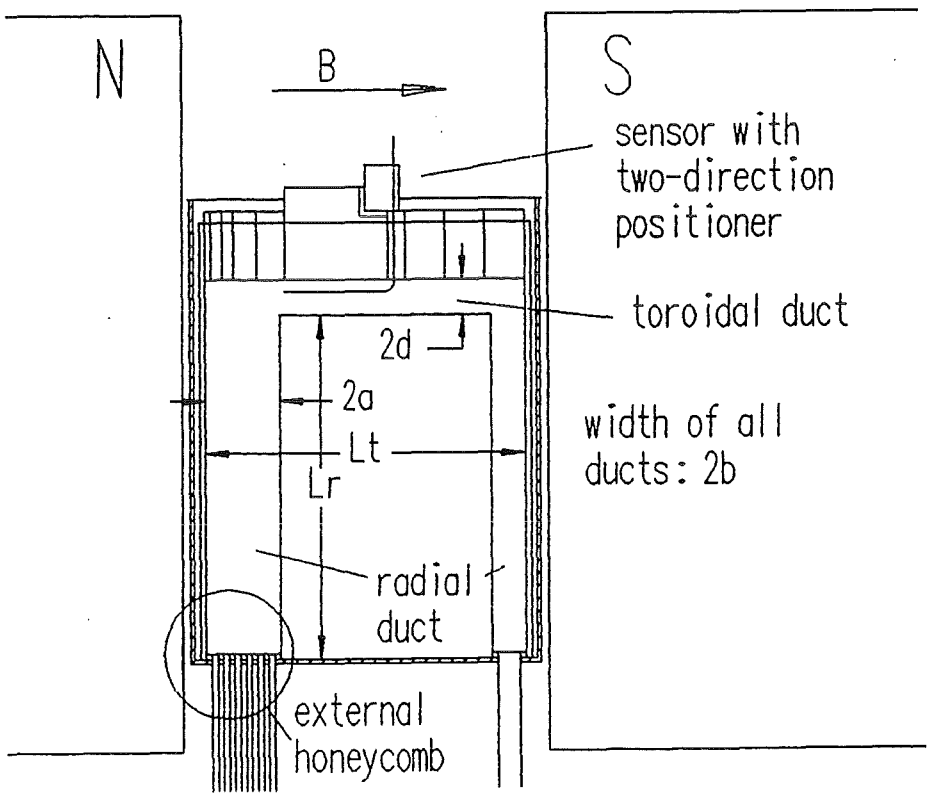

Fig. 2.1 Schematical graph of test section for the experiments with the bend partly parallel to the magnetic field B (bpaB-exps)

In order to generate a constant velocity in the inlet cross section a flow straightener was used consisting of a bundle of plastic tubes. The test section casing had electrically insulating inner walls and the dimensions $2a=40$ mm in the inlet radial channel, a height 2d of 19 mm in the toroidal part and $2a_0=20$ mm in the outlet radial channel. The width of the U-bend was $2b=40$ mm. Thin electrically conducting walls were obtained by glueing sheets of stainless steel of thicknesses $t_W=1$ mm on the walls of the casing, reducing the characteristic lengths given above. In most of the experiments a symmetric U-bend was investigated (Geometries B, C, D) by using a plexiglass insert to reduce the depth of the inlet radial channel. In Geometry C the stainless steel sheet at the FW was replaced by a brass sheet of the same thickness which results in a FW conductivity higher by more than a factor of 10. In Geometry D the metal sheets were removed and the velocity distribution in a nonconducting U-bend was investigated. Table II.I contains the values of the characteristic lengths, the wall conductance ratios C, and the maximum Hartmann numbers and Interaction parameters N which are defined with the half depth "a" of the inlet dimension in direction of the magnetic field:

$$C=t_W\sigma_W/(a\sigma),$$
$$Ha=aB(\sigma/(\rho\nu))^{0.5}$$
$$N=a\sigma B^2/(\rho\bar{v}),$$

where σ_W and σ are the specific electric conductivities of the wall material and mercury ($\sigma_{wss}=1.16\cdot10^6$ A/Vm; $\sigma_{W\ brass}=1.5\cdot10^7$ A/Vm, $\sigma_{Hg}=1.06\cdot10^6$ A/Vm), ρ and ν are the liquid metal density and kinematic viscosity ($\rho_{Hg}=1.357\cdot10^4$ kg/m^3, $\nu_{Hg}=1.2\cdot10^{-7}$ m^2/s), and $\bar{v}$ is the cross sectional averaged liquid metal velocity in the inlet radial channel.

Table II.I Test section characteristics for the experiments with the bend partly parallel to B (bpaB-exps)

Geometry	a (mm)	(mm)b	2d (mm)	a_o (mm)	C*	Ha_{max}*	N_{max}*
A	19	19	17	9	0.06	≈460	≈70
B	9	19	17	9	0.122	≈230	≈75
C	9	19	17	9	0.122**	≈230	≈35
D	10	20	19	10	0	≈255	≈150

$L_r\approx210$ mm, $L_t\approx130$ mm (for A: $L_t=148$)
* values based on the quantities in the radial channel
** except wall conductivity at First Wall which is $C\approx1.2$

The aim of the experiments was to create a data basis for a wide range of Hartmann numbers and Interaction parameters.

The top wall (FW) of the toroidal section consisted of plexiglass pieces (covered on the liquid metal facing side with the appropriate metal sheets). One of these pieces contained the velocity probe which could be traversed in the y and z directions, see Fig. 2.1. By mounting the instrumented part at different positions in the toroidal channel different values of the coordinate x were obtained.

For the experiments with the bend perpendicular to B (bpeB-exps), the test section was rotated horizontally by 90°. Compared to the precedent bpaB experiments the test section inserts were modified as shown in Fig. 2.2 and Table II.II. The experiments with nonconducting walls were performed with a sharp-edged and a rounded corner. In the experiments with conducting walls only the sharp-

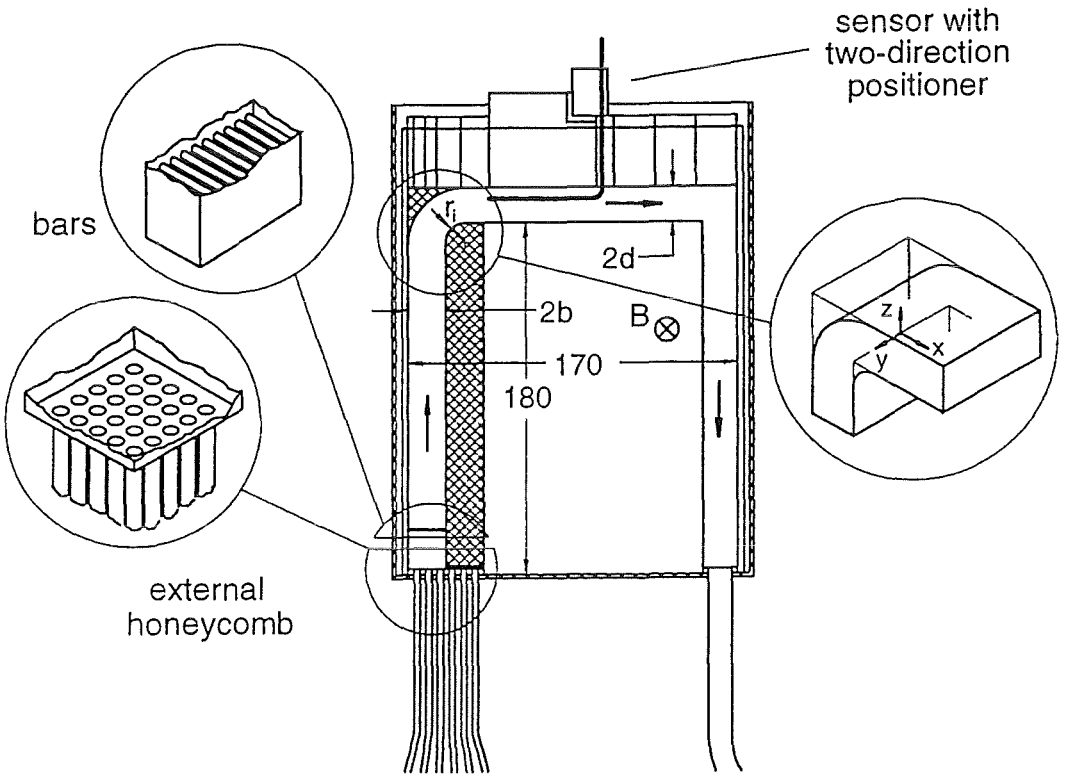

Fig. 2.2 Schematical graph of test section for the experiments with the bend perpendicular to B (bpeB-exps)

edged version was used, however, two different wall conductance ratios were investigated.

Note that Ha, N and C are always defined with the half length "a" of the inlet duct in direction of B. Therefore "a" (and with this "b") are defined differently in the two types of experiments.

Table II.II Test section characteristic for the experiments with the bend perpendicular to B (bpeB-exps)

	nonconducting bend	conducting bend
C	0	1.0; 0.1
a(mm)	20	19.5
b(mm)	10	9.5
d(mm)	8.5	8.0
r_i(mm)	0; 10	0
r_a(mm)	0; 30	0
Ha	25 - 630	
N	0.02 - 230	
Re	$2 \cdot 10^4$ - $3.5 \cdot 10^5$	

2.2 Measuring Techniques for Local Velocities

2.2.1 Hot Wire Anemometry

Electric potential probes cannot be used in the bpaB-exp to measure the velocity component u in the toroidal duct because u is parallel to B. Hot wire anemometry was believed to be best suited for this purpose. However, the use of this technique in mercury and magnetic fields requires a much larger technological and experimental effort compared to conventional applications. Figure 2.3 shows the hot wire probe used in the present experiments. The tungsten wire (thickness 5 µm) was electrically insulated by a SiO_2 layer (thickness 5 µm) which subsequently was covered by a thin Cr layer, followed by a gold layer of 2 µm thickness in order to ensure good wetting and to avoid the adherence of impurities. An accurate temperature stabilization of the loop was required and a procedure to compensate the small residual temperature changes.

Another MHD feature which might falsify the measurements is the existence of flow regions with reduced velocities upstream of a body located in a flow parallel to the magnetic field /16,17/. The dimensions of these regions are dependent on Ha and N based on the dimensions of the body. Table II.III contains characteristic values for the used probe. Figure 2.4 shows the decrease of the velocity for different distances x/d and Hartmann numbers. It was estimated for the present experimental conditions that these effects could cause an error less than 5 %.

Special attention was paid on the hot wire calibration at low velocities. First, an insert containing a venturi nozzle with a manometer for pressure difference measurement was used, see Fig. 2.5a Due to an unsufficient accuracy in the low ve-

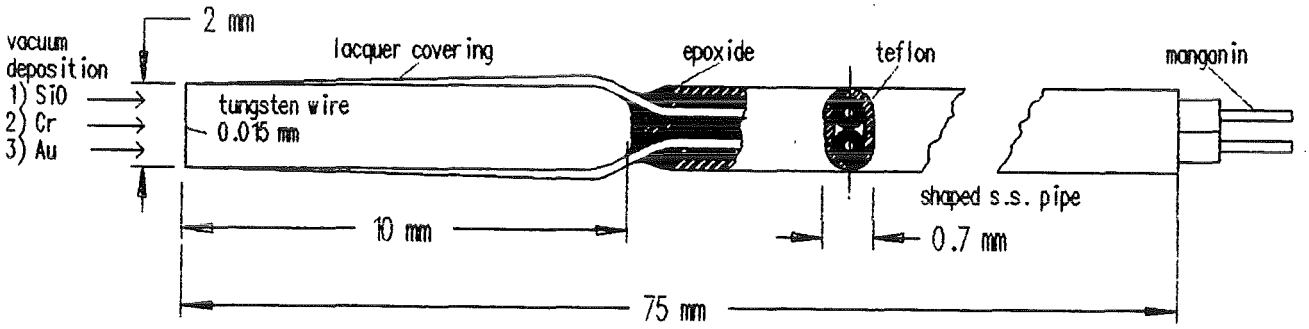

Fig. 2.3 Hot wire probe

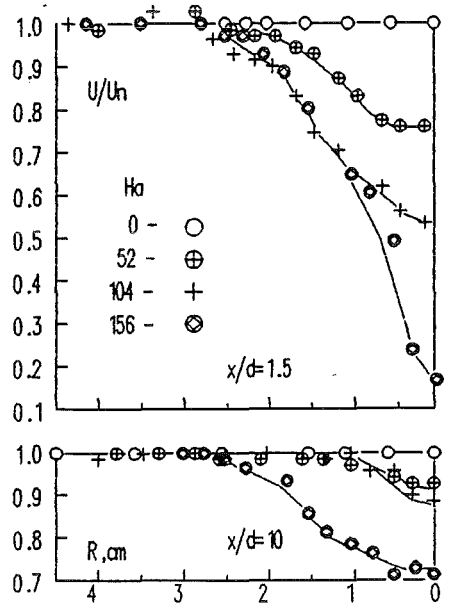

Fig. 2.4. Decrease of velocity in upstream region (from /17/)

Table II.III Ha and x/d for hot wire probe components

	Ha	x/d
wire	0.22	1
probe body	10	29
probe rod	31	40

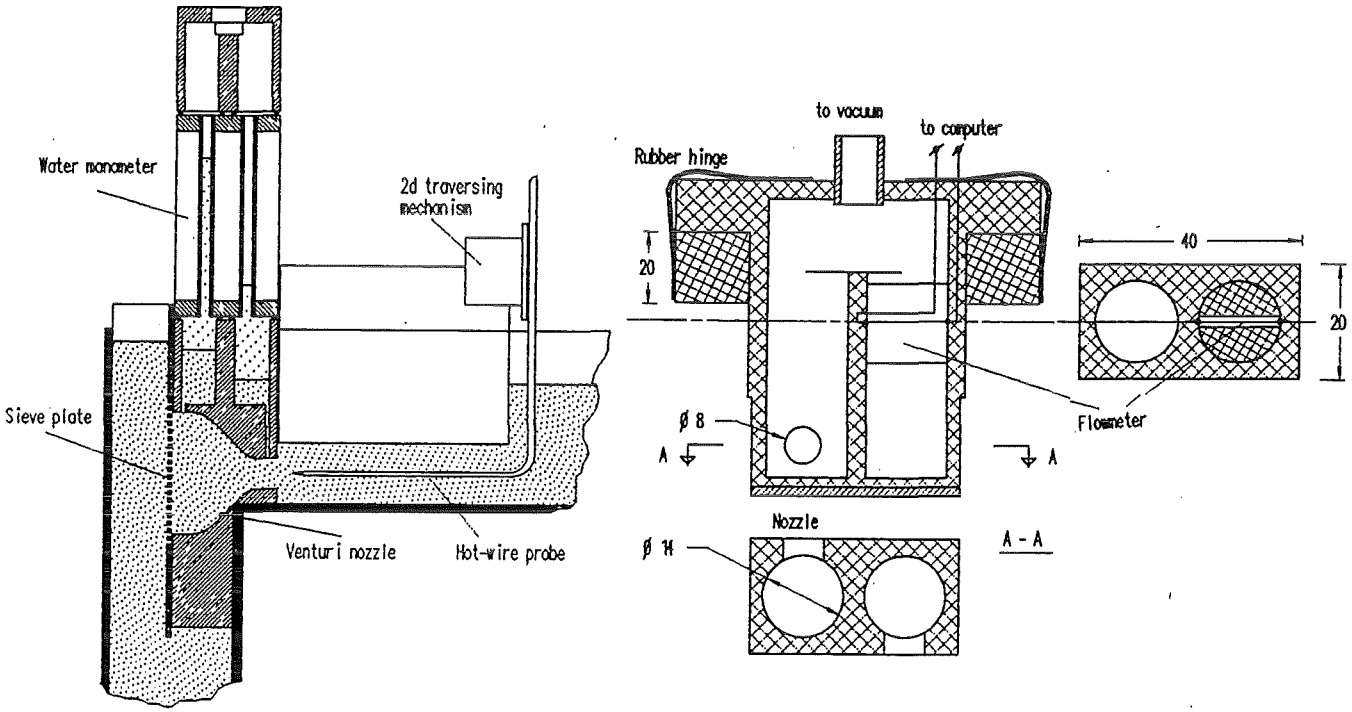

a) first calibration insert b) second improved calibration insert

Fig. 2.5 Inserts for hot wire calibration

locity range this unit was replaced by the improved system shown in Fig. 2.5b consisting of a nozzle and an integrated EM flow meter. The calibration runs were performed at a maximum field strength of $B \approx 1$ Tesla at which most of the experiments were performed, as required by /18/.

The velocity distribution in the nozzle jet was determined by traversing the probe and appropriate wire positions were determined where the velocity profile was quite flat. The Figs. 2.6 and 2.7 show measured velocity distribution and a calibration curve.

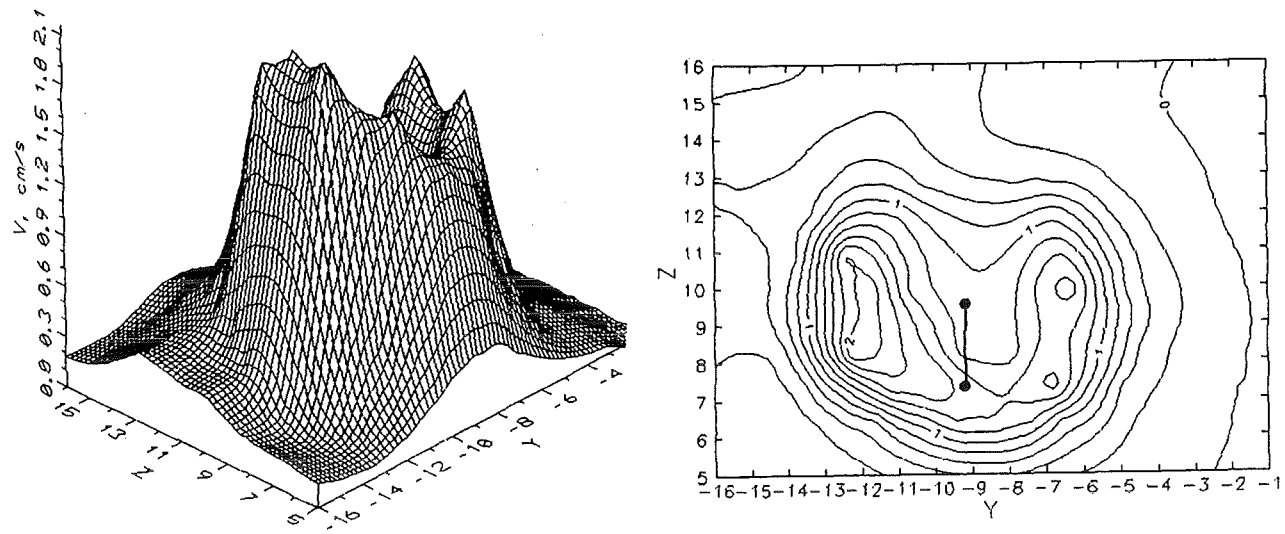

Fig. 2.6 Velocity distribution for a nozzle flow of $\bar{v} \sim 1.1$ cm/s (B = 1 Tesla)

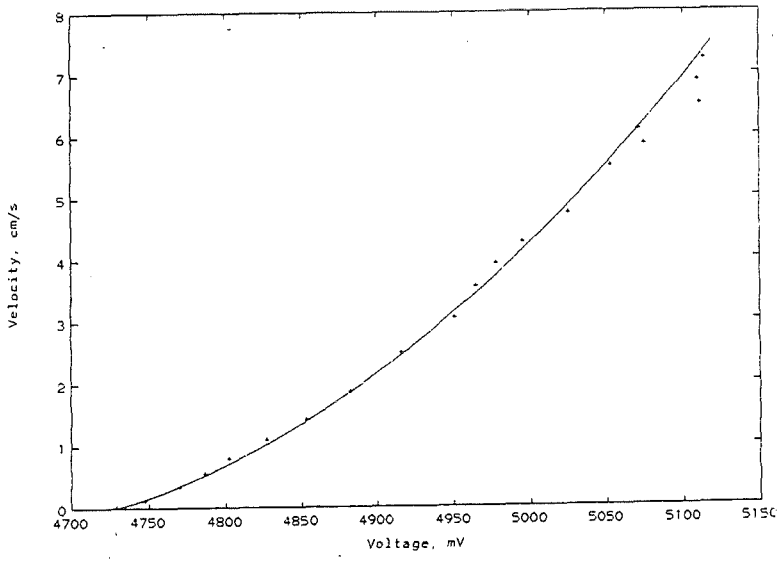

Fig. 2.7 Characteristic hot wire calibration curve (B = 1 Tesla)

2.2.2 Electric Potential Probes

These probes are widely used in MHD flow. The measured electric potential differences $\partial\Phi/\partial z$ and $\partial/\Phi\partial x$ between the probe tips perpendicular to B are proportional to the velocity components u and w as long as the electric currents j_z and j_x between the probe tips is negligible, (for coordinates, see Fig. 2.8), as can be easily seen by Ohm`s Law

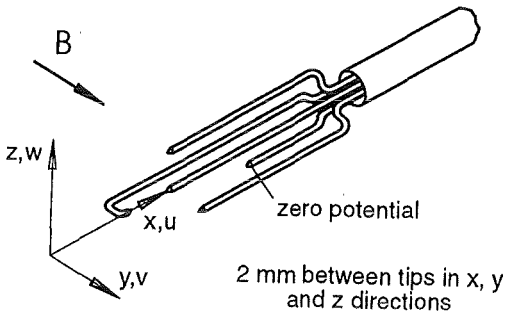

a) Single-Triple Probe (STP)

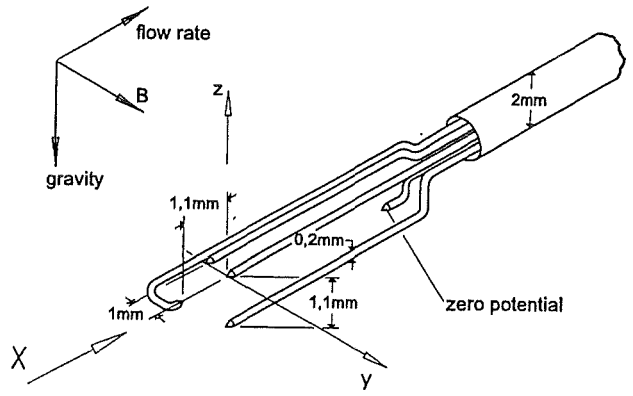

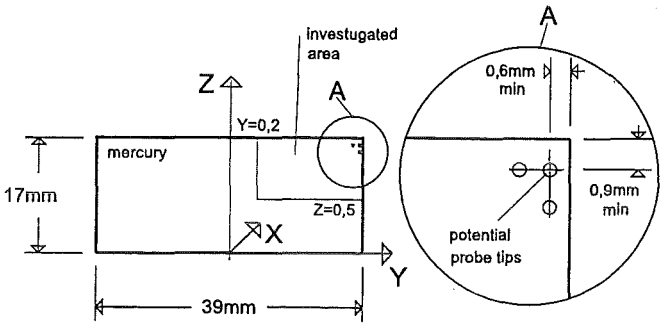

Dimensionless dimensions: X=x/20mm; Y=y/19.5; Z=z/17.
For Ha and N - a=20 mm.

b) STP for measurements close to the wall

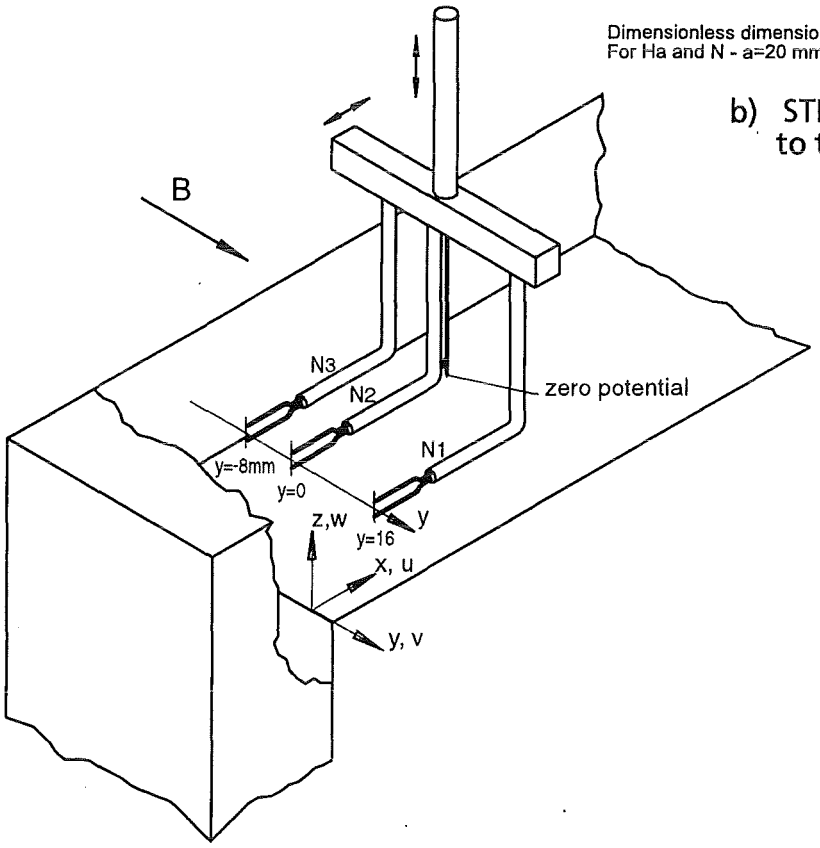

c) Triple-Single-Probe (TSP)

Fig. 2.8 Traversable potential probes

$$u = j_z + \partial\phi/\partial z; \quad w = j_x - \partial\phi/\partial x.$$

For insulated duct walls this assumption is justified. For well conducting duct walls ($C >> Ha^{-1}$) the currents are in the order of C. For the bpeB-exp with $C = 1$ (compare Table II.II) the currents reach the same order as the other terms.
Therefore, these results are considered to be of rather qualitative nature. For the other versions with conducting walls, the values of C are so small that the assumption is fairly well fulfilled.

Beside several standard electric potential probes consisting of one pair of electrodes, two other types of traversable probes were used (Fig. 2.8):

- Single-Triple-Probes (STP), which measure simultaneously the potential gradients in the x,y and z directions (Fig. 2.8a). The STP with the small tip distances (Fig. 2.8b) was built for the final bpeB-exp with $C=0.1$ where the aim was to measure very close to the wall.
- The Triple-Single-Probe (TSP) which measures simultaneously potential gradients $\partial\phi/\partial z$ at three different positions y in the test section (Fig. 2.8c). The correlation of these signals provide information on the two-dimensionality of the flow structure in planes perpendicular to the magnetic field B.

2.3 Data Acquisition

During the experiments, the following quantities were measured: flow rate Q, magnetic field strength B, velocity probe signals and the position of the probe tip. In the bpaB-exps, the probe signals were taken sequentially with a frequency of 200 Hz for a measurement period of 20 s for each probe position. For the subsequent bpeB-exps the capacity of the computerized data acquistion system was considerably enlarged: all probe signals were measured in parallel with 200 Hz for 150 s.

3. THEORETICAL ANALYSIS

3.1 Velocity Distributions in U-bends Partly Parallel to the Magnetic Field (bpaB-exps)

The flow in a U-bend has been analysed by the asymptotic theory for high values of Ha and N . The governing equations and boundary conditions are given in detail in Ref. /12/. The assumptions used to simplify the analysis are the following: i) the induced magnetic field may be neglected compared to the external magnetic field (small magnetic Reynolds number), ii) $Ha >> 1$, $N >> Ha^{3/2}$, $C >> Ha^{-1/2}$, iii) radial ducts are semi-infinite, so that the flow is fully developed as $z \rightarrow -\infty$. The assumptions ii) allow to neglect inertia terms everywhere, while viscous effects will be confined to thin boundary layers at the wall (Core Flow Approximation (CFA) method).

At high Hartmann numbers the flow region exhibits inviscid cores CR and CT, Hartmann boundary layers (H) near the walls perpendicular to the magnetic field with a thickness $O(Ha^{-1})$, parabolic layers SR, ST, F, S and I of $O(Ha^{-1/2})$ at the walls parallel to the magnetic field, corner layers A1 and A2 with dimension $O(Ha^{-1/2})x(O(Ha^{-1/2})$ see Fig. 3.1. Under the assumptions made, the problem is reduced to a system of two-dimensional equations governing the wall potentials and the core pressure in the radial duct. All other variables both in the core and in the layers are expressed in terms of them. The main flow features, which result from this

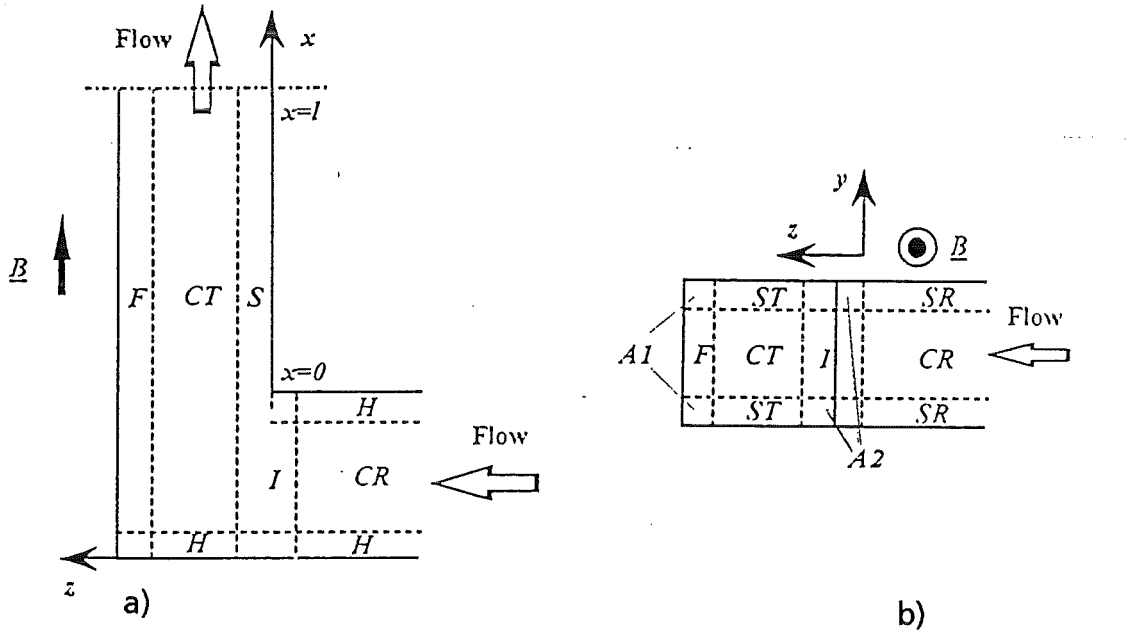

Fig. 3.1 Flow subregions at high Ha and N

model are the following: In the radial duct close to the junction the fluid is pushed towards the sidewalls and part of the core flow enters the layers SR. At the junction these layers carry for the present Geometry B, see Table II.1, 18% of the total volume flux. In the toroidal duct the fluid participates in a very complex motion which involves helical-type of flow. The core of the toroidal duct CT does not carry volume flux in the x-direction, so that all the volume flux is carried by the layers ST, F, I and S. The flow distribution between the layers is given in Table III.I. However, the core CT is not completely stagnant, since both core velocity components perpendicular to the field are not zero. They are responsible for a flow distribution between the parabolic layers. The projection of the helical flow on the y,z-plane in the toroidal duct results in two vortices with the velocity component in the center towards the FW in the first part of the U-bend and opposite in the second part. The fluid that enters the layers F or SR from the core returns back within these layers and the layer S (Fig. 3.2). It should be noted, however, that the flow pattern in the toroidal duct is essentially three-dimensional with maximum absolute core velocity close to the Hartmann walls (20 % of the average velocity in the radial ducts) and zero at the symmetry plane x=I. The reversed flow in the layer S (Table III.I) is associated with a three-dimensional vortex close to the symmetry plane (for details see /12/).

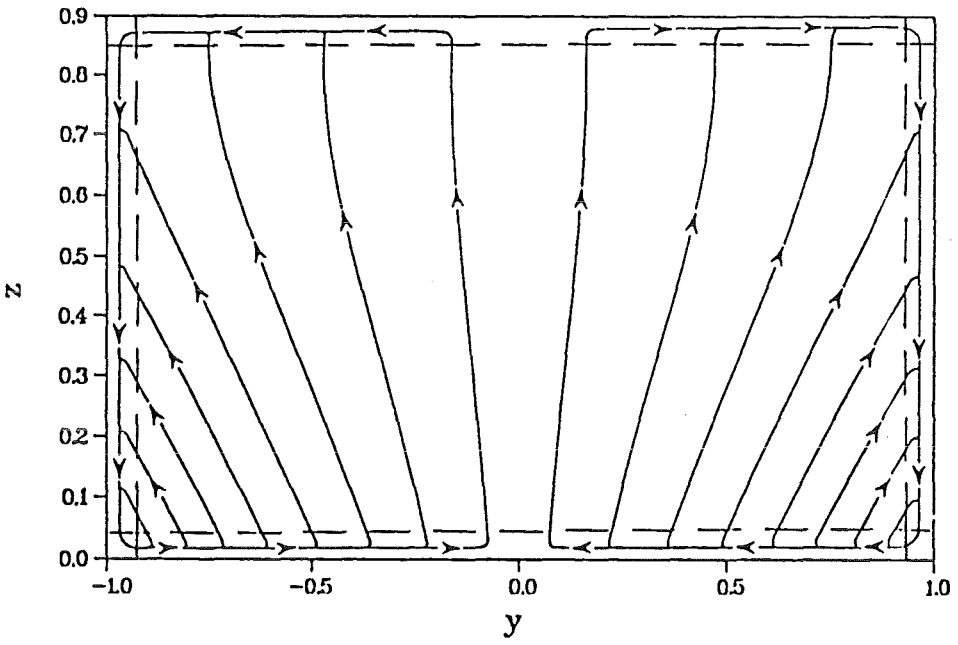

Fig. 3.2 Projections of streamlines in the toroidal duct on (y,z)-plane at x=I

Table III.I Flow distribution between the layers in the toroidal duct (Geometry C, flow rates normalized with total flow rate Q)

x	Q_F	Q_{ST}	Q_S
0	22.9%	52.6%	24.5%
$l=(L_t-2a)/2$	47.1%	65.3%	-12.4%

3.2 Velocity Distribution in Bends Perpendicular to the Magnetic Field (bpeB-exps)

The asymptotic theory for high Ha and N (CFA) has been also used for this flow geometry /19/. Figure 3.3 shows the results for a nonconducting bend: the velocity distribution is similar to that of a potential flow with the highest velocity near the inner corner (for the calculations a small inner radius was assumed). As normalizing quantities, the cross section averaged velocity is used for the velocity and the quantity "a" for the coordinates.

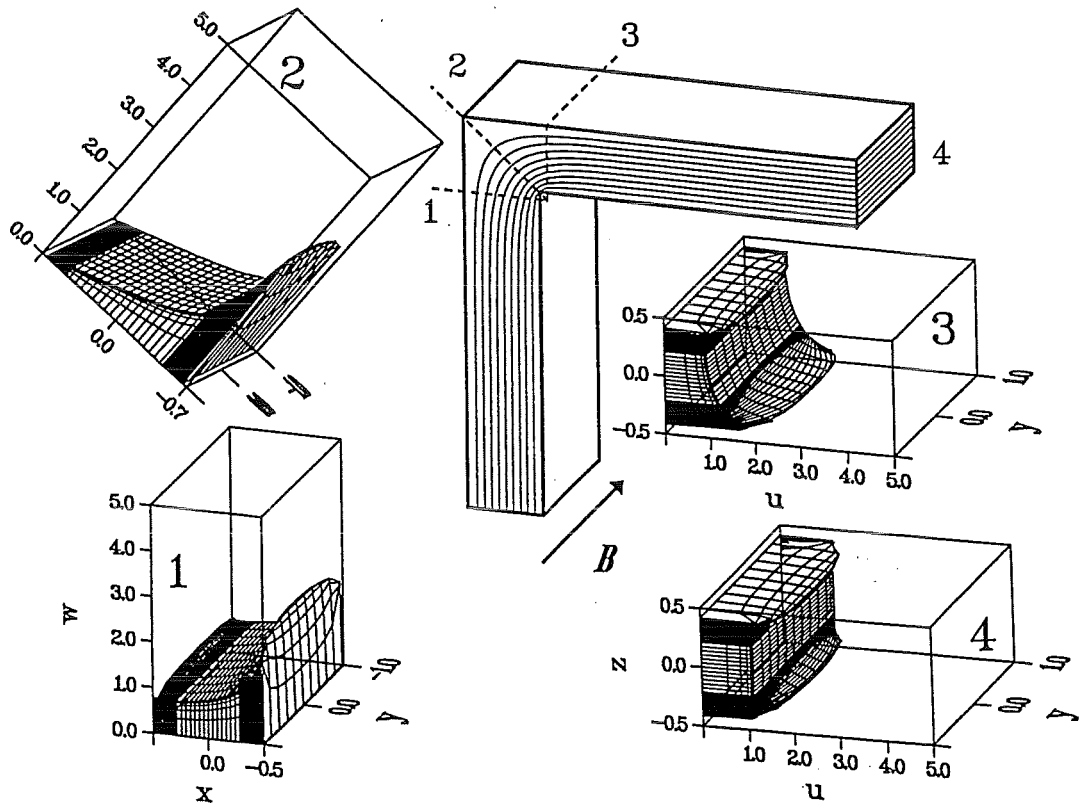

Fig. 3.3 Calculated velocity distribution in a nonconducting bend (Ha = 500, N→∞)

For the conducting bends (Fig. 3.4) an expressed M-shaping is observed near the walls parallel to B. The symmetric profile in the inlet duct deforms in the turning zone in such a way that a strong velocity jet occurs close to the inner corner. Downstream of the bend again a symmetric M-shape profile starts to develop.

Increasing the wall conductivity, the M-shaping first increases, reaches a maximum and almost disappears for highly conducting duct walls. The M-shaping for the two considered values of the wall conductance ratio does not differ very much although C differs by one order of magnitude. The reason for this is that the maximum velocity scales as

$$u_{max} \sim (C + Ha^{-1})\ (1 + C)^{-1}\ (C + Ha^{-0.5})^{-1}.$$

The differences of the electric currents within the flow are quite significant because

$$j \sim (C + Ha^{-1})\,(1 + C)^{-1}.$$

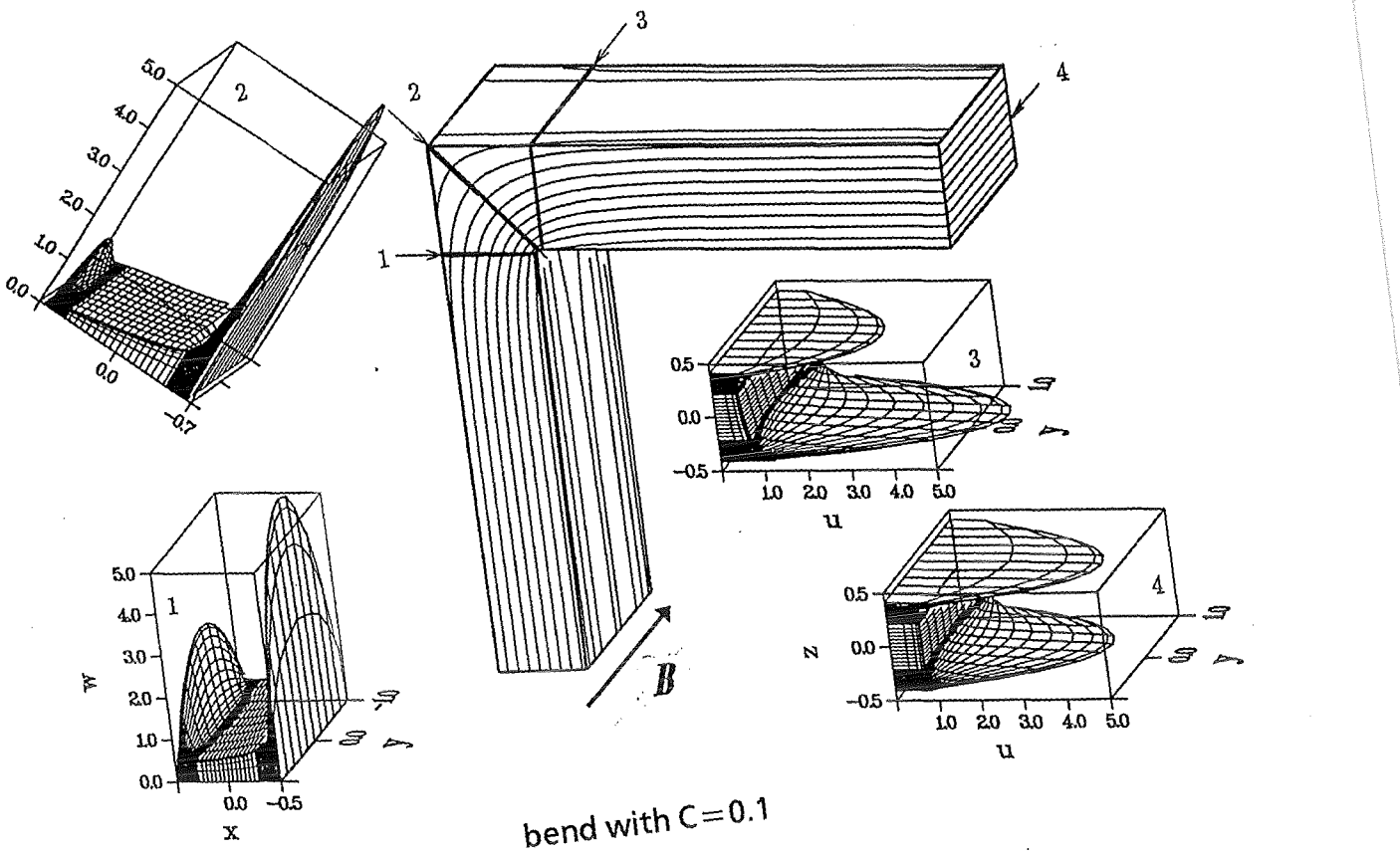

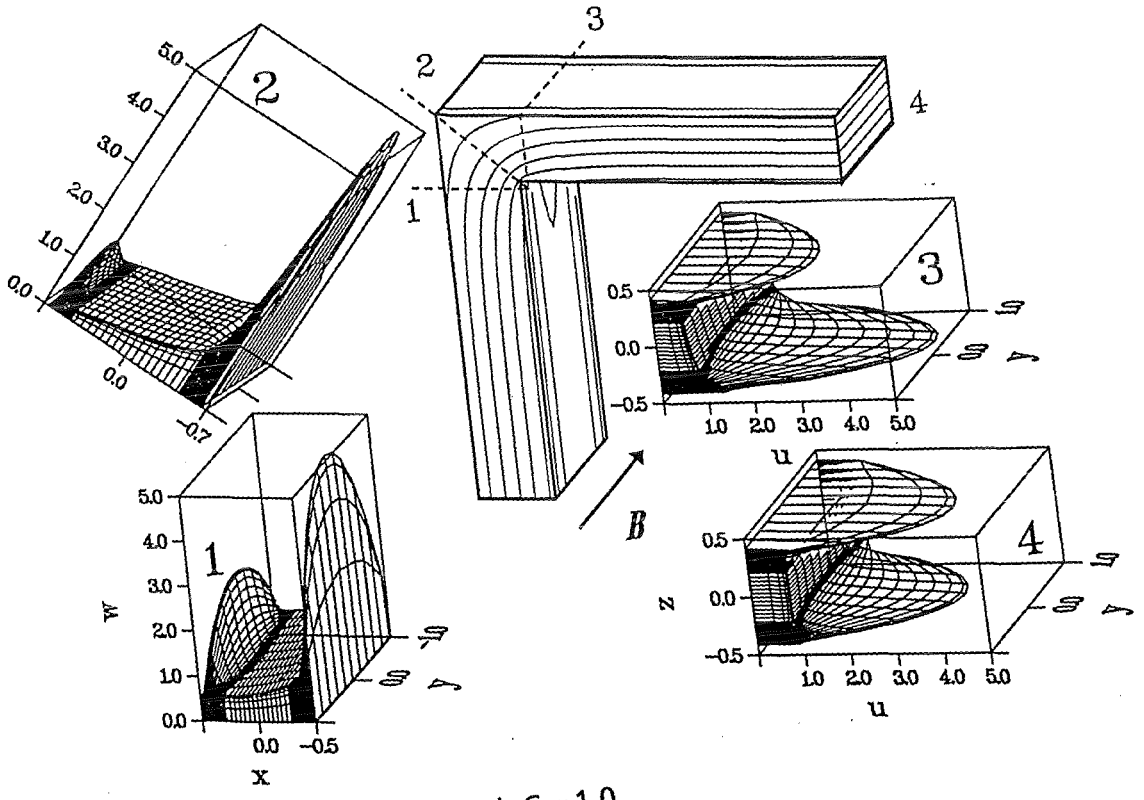

Fig. 3.4 Calculated velocity distributions for conducting bends (Ha=500,N→∞)

4. EXPERIMENTAL RESULTS

The results for the two different types of experiments are presented in Sections 4.1 and 4.2. The same coordinate system is used but the direction of the magnetic field differs, see Fig. 4.1. All velocities and velocity fluctuations are normalized with the corresponding cross section averaged throughput velocities. The values for x,y are normalized with the inlet duct half lengths in corresponding directions , z is normalized with "2d".

The experiments concentrated in both cases on the flow structure in the vicinity of the first 90° bend.

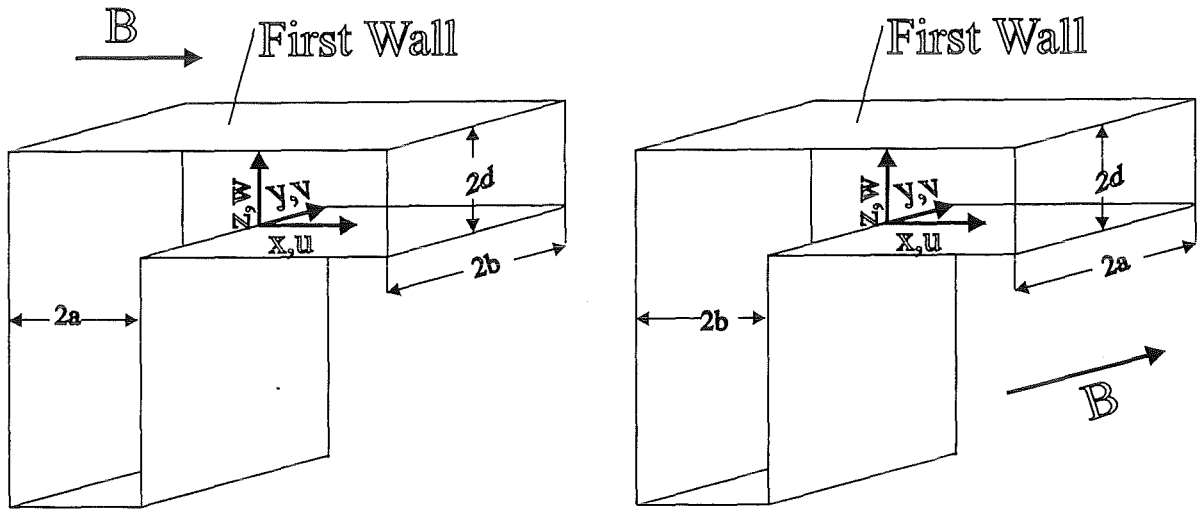

bpaB-experiments bpeB-experiments

Fig.4.1 Coordinate system

4.1 Bend Partly Parallel to B (bpaB-exps)

4.1.1 Velocity Distribution in the Radial Duct

A simple traversable potential probe was used which measured only the velocity component in z-direction. Figure 4.2 shows the distribution of the mean velocity for the duct with thin conducting walls. For Ha=46 and N=0.2 the MHD influence is not very expressed; a quite flat velocity distribution is observed. For the higher values of Ha and N a characteristic M-shaped profile exists. It should be taken into account that very close to the sidewalls the velocities could still in-

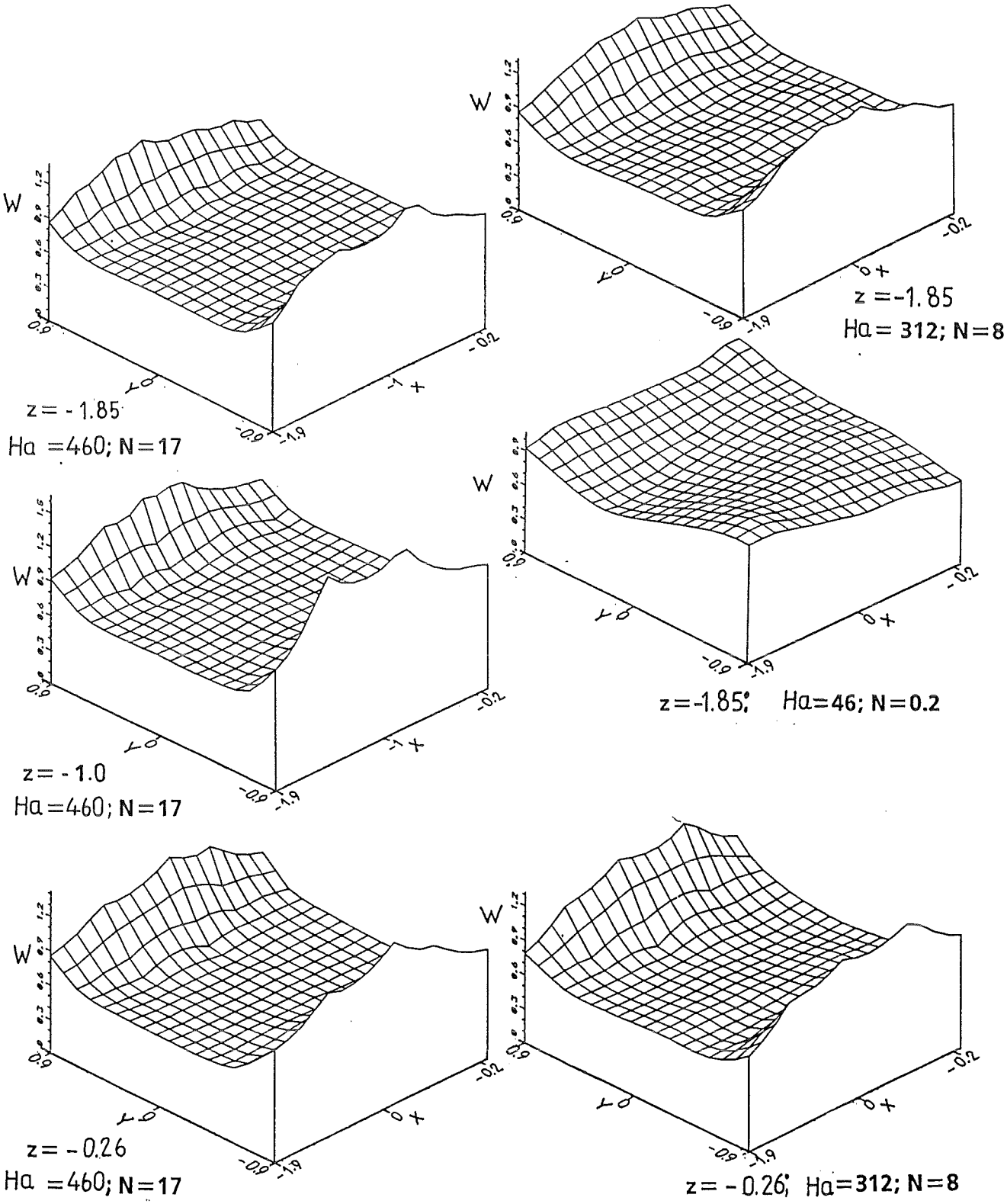

Fig. 4.2 Velocity distribution in the radial duct for C = 0.06 (potential probe)

crease considerably. These layers with increased velocity are very important for the flow phenomena in the toroidal duct as discussed later. As outlined in Section 3, the 3d electric currents due to the flow deflection into the B direction should increase the M-shaping when approaching the bend. This effect is not very pronounced in the experiments and might be hidden by the fact that the thickness of the sidelayers at z= -2 is already considerably thicker than predicted for laminar flow. This might be caused by an intense mixing effect due to turbulence as shown in Fig. 4.3 which contains the corresponding distributions of the velocity fluctuations. For the lowest values of Ha and N again a quite flat distribution is observed whereas for the highest values the fluctuations are significantly larger in the zones where the gradients of the mean velocities are largest.

For nonconducting walls (Fig. 4.4) the influence of the downstream bend due to 3d currents is much more expressed: a strong redistribution is observed for $z = -0.26$, again pushing the liquid towards the side walls. This tendency was also observed for other flow conditions (e.g. changing magnetic field strength in straight ducts /17/). The turbulence level increases also near the side walls with decreasing z. For the smallest value of z, the values in the middle of the duct are also increased, this complex behaviour will be explained in the next sections.

4.1.2 Velocity Distributions in the Toroidal Duct

The Figs. 4.5 - 4.11 show results obtained with the hot wire probe. In order to interpretate these signals one should keep in mind that the hot wire is mainly sensitive to the absolute velocity perpendicular to the wire. During the planning of these experiments it was assumed that in the toroidal duct the flow direction is parallel to the x direction. This assumption is not justified as shown in the following. Therefore, the velocity determined from the hot wire signal may contain the velocity components w if the wire is parallel to the y-direction and the velocity component v if the wire is parallel to the z-direction. For the results shown in Figs. 4.5-4.7, the wire was parallel to y.

Fig. 4.5 shows the influence of Ha and N for the duct with thin conducting walls. For pure hydrodynamic flow (Ha=N=0) a characteristic separation zone occurs - as expected - downstream of the inner corner. For the values of Ha = 230 and N = 17, MHD effects are sufficiently large to suppress this recirculation zone. The velocity distribution for Ha=230 and N=35 differs significantly from the other ones: in agreement with the theoretical analyses for high Ha and N (compare Sec-

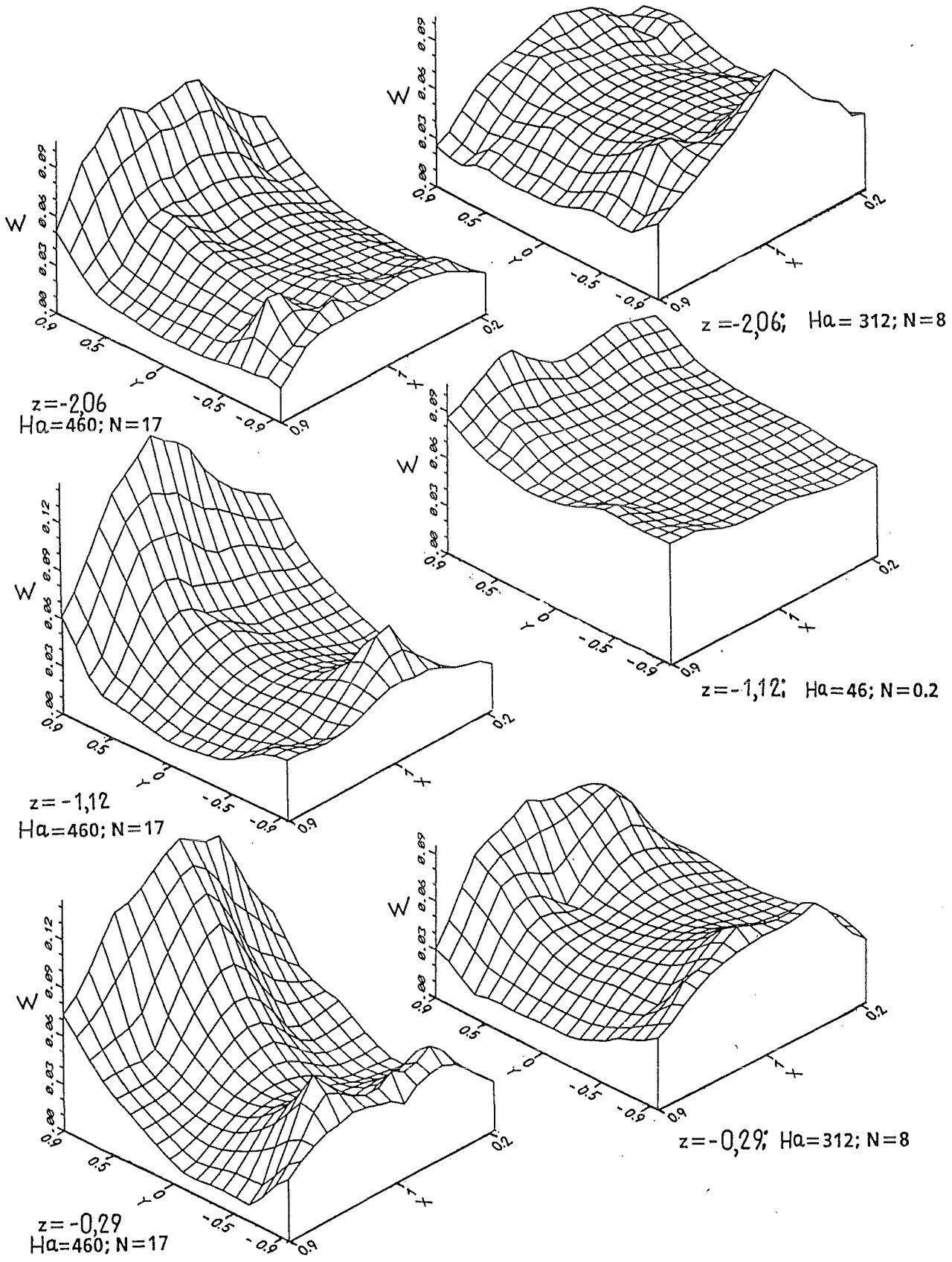

Fig. 4.3 Velocity fluctuations in the radial duct for C = 0.06 (potential probe)

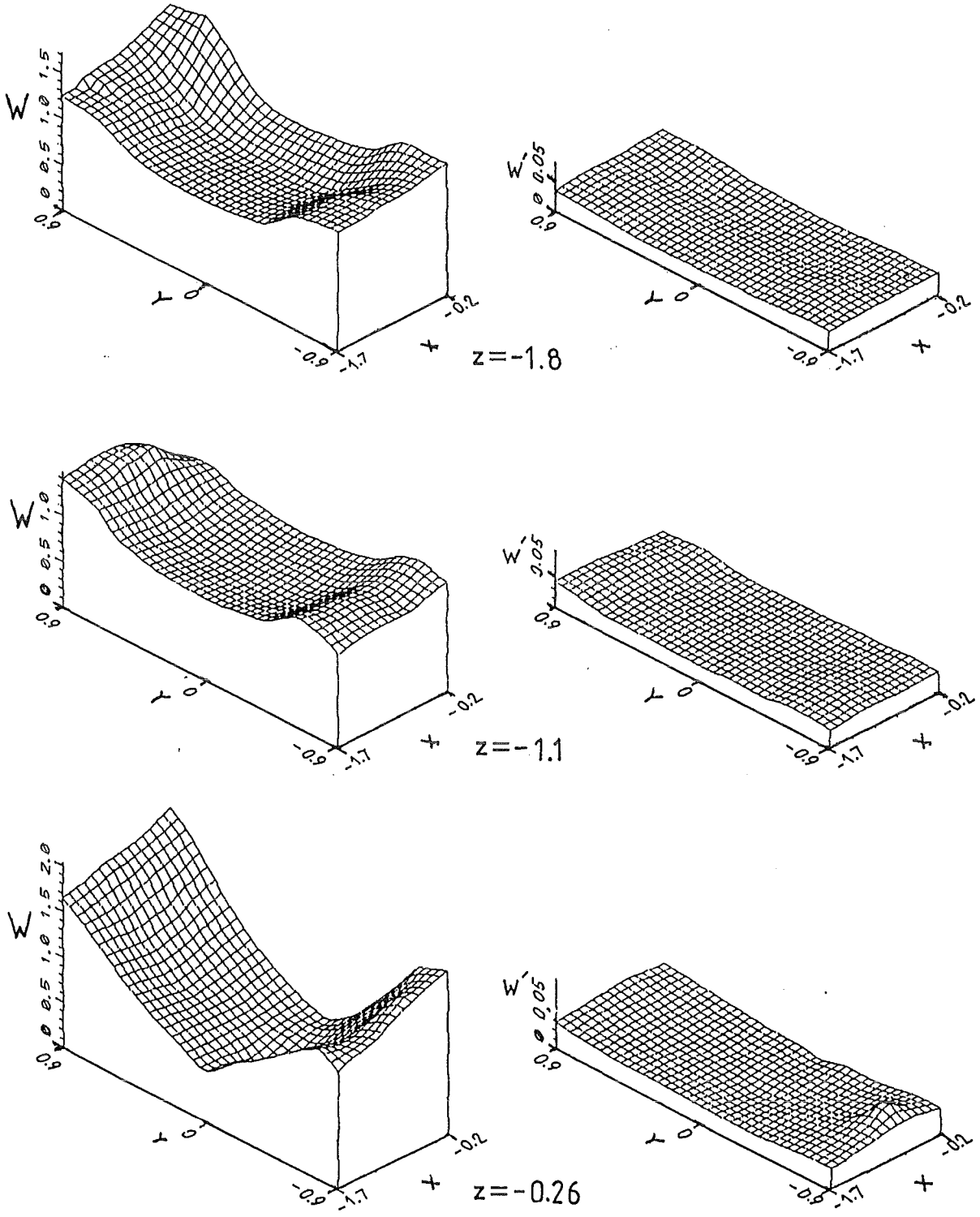

Fig. 4.4 Velocity and velocity fluctuations in the radial duct for C=0, Ha=255 and N=17 (potential probe)

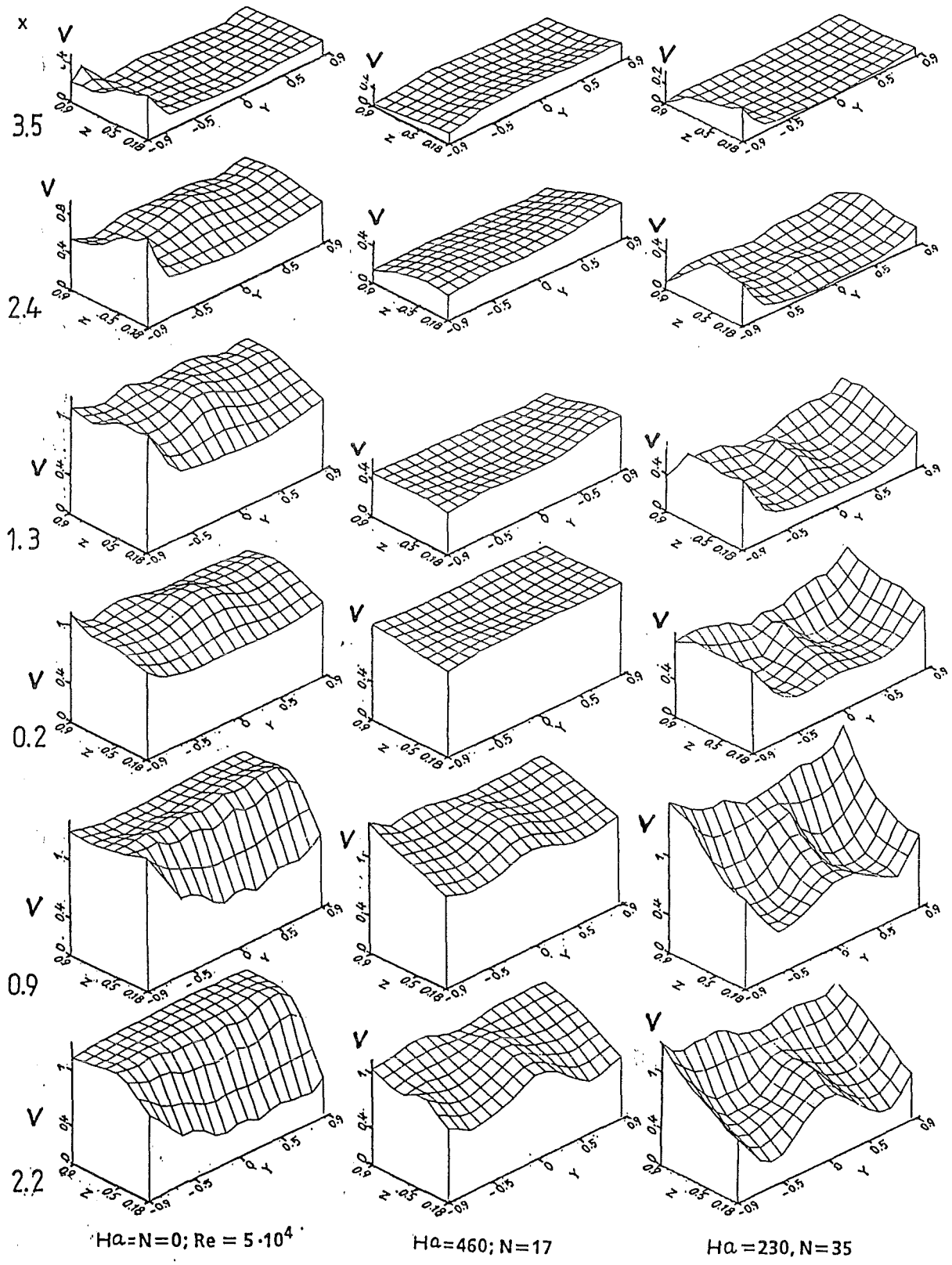

Fig. 4.5 Velocity distribution in the toroidal duct for C=0.06 (hot wire probe)

tion 3) the liquid metal flow is pushed towards the side walls with a distinctively higher velocity at the FW than at the Second Wall ($z=0$). Surprisingly, there is an expressed maximum at $y \approx 0$ which is not predicted by theoretical analyses.

Figure 4.6 contains the corresponding results for the velocity fluctuations. For pure hydrodynamic flow the fluctuations are quite uniform and small except in the separation zone. For the larger values of Ha and N the distributions differ significantly. For $x<0$, strong fluctuations occur close to the side walls and in the middle of the duct ($y \approx 0$). For $x>0$, the fluctuations in the middle of the duct have increased.

Figure 4.7 contains mean velocity distributions for Geometry B. The spatial resolution is higher compared to Figs. 4.5 and 4.6 due to an increased number of measurement positions. Again, high velocities in the side layers are found and the characteristic maxima at $y \approx 0$.

One explanation for these surprising velocity distributions is the occurence of two strong vortices with axes parallel to B. Such vortices are generally favourized in MHD flow due to small damping, compare /20/. Such vortices were also predicted by analyses for inertialess MHD flow (Section 3), however, with maximum vortex velocities in the core of about 10 % of the cross section averaged velocity. These values are significantly smaller than the experimental values. The observed high turbulence levels also indicate that the flow behaves differently from that predicted by the CFA.

If such strong vortices exist in the toroidal duct then one would expect that the hot wire probe signals differ characteristically if the wire orientation is changed. Figure 4.8 shows results for a hot wire parallel to z: the mean velocity is still the highest in the side layers and the maximum at $y \approx 0$ still exists. This result rather indicates a jet type flow distribution than a vortex flow. (However, a jet at $y \approx 0$ is in contradiction with basic MHD considerations).

Comparing in more detail the velocity distributions in the entrance zone of the toroidal duct ($x<0$) one observes for the wire parallel to z higher velocities near the FW. This could be caused by higher velocity component in y direction, characteristic again for a vortex flow. The velocity fluctuations first occur close to the FW and expand in the core region with increasing x.

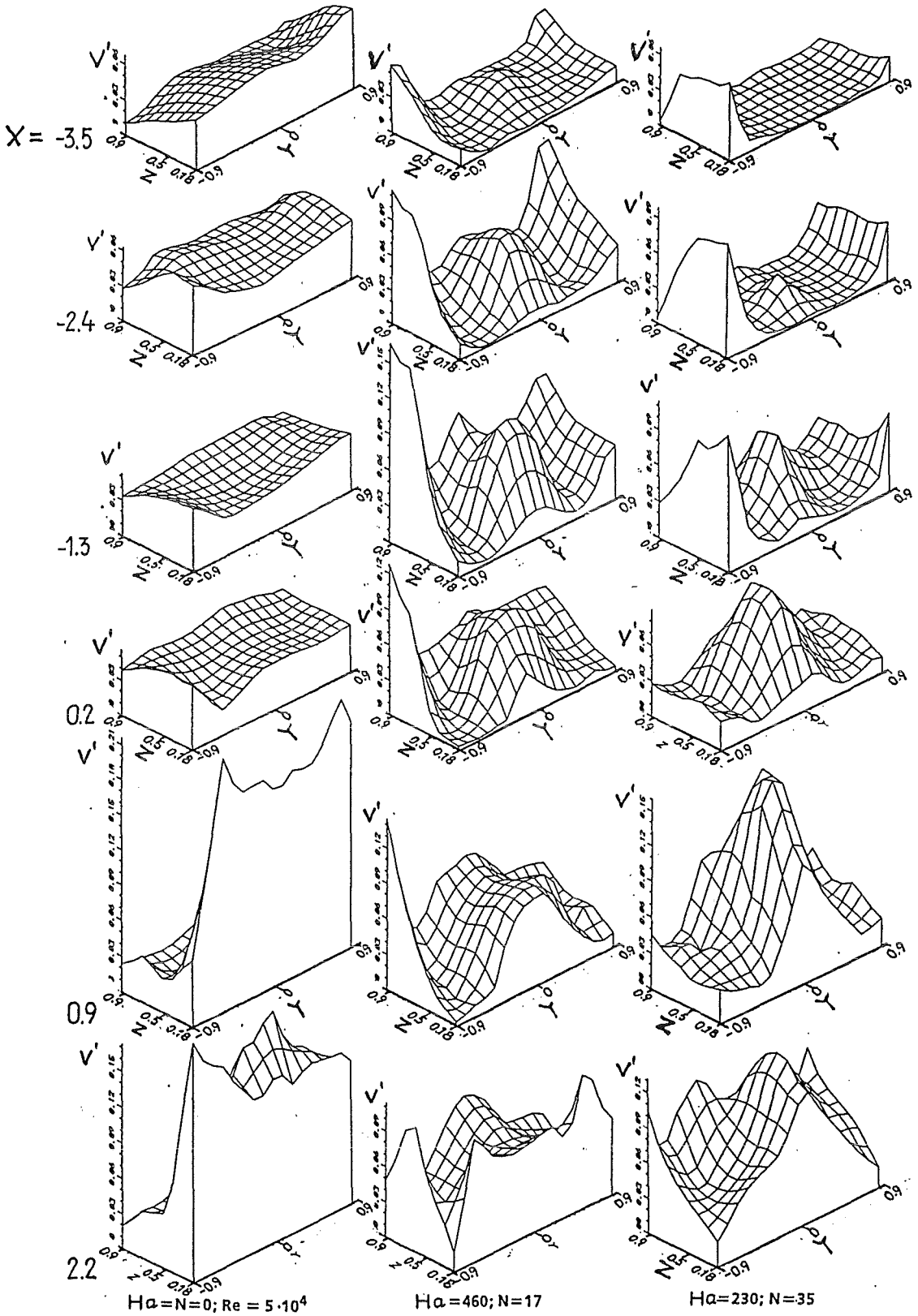

Fig. 4.6 Velocity fluctuations in the toroidal duct for C=0.06 (hot wire probe)

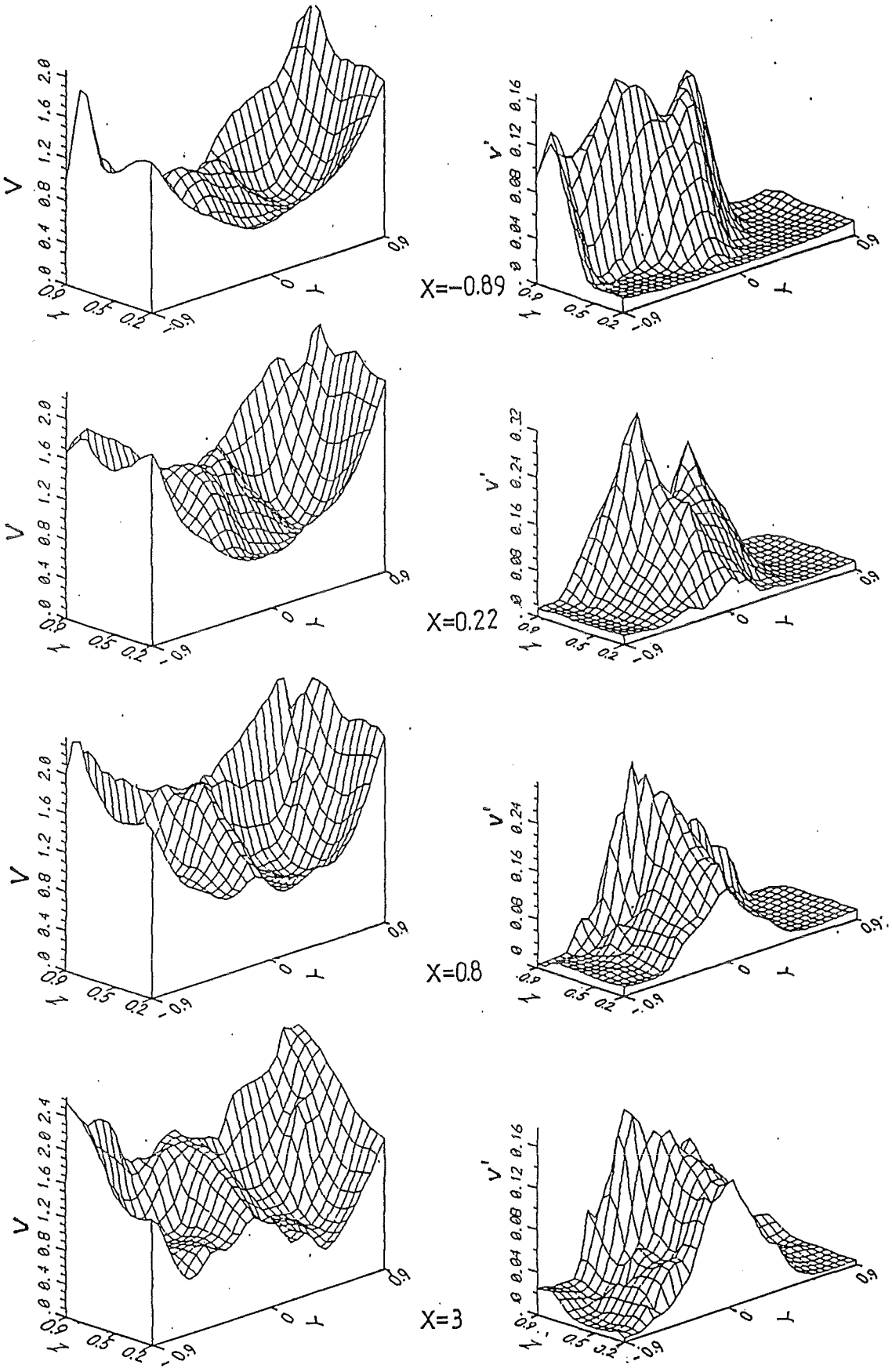

Fig. 4.7 Velocity and velocity fluctuations for C=0.122, Ha=230 and N=35; (hot wire probe)

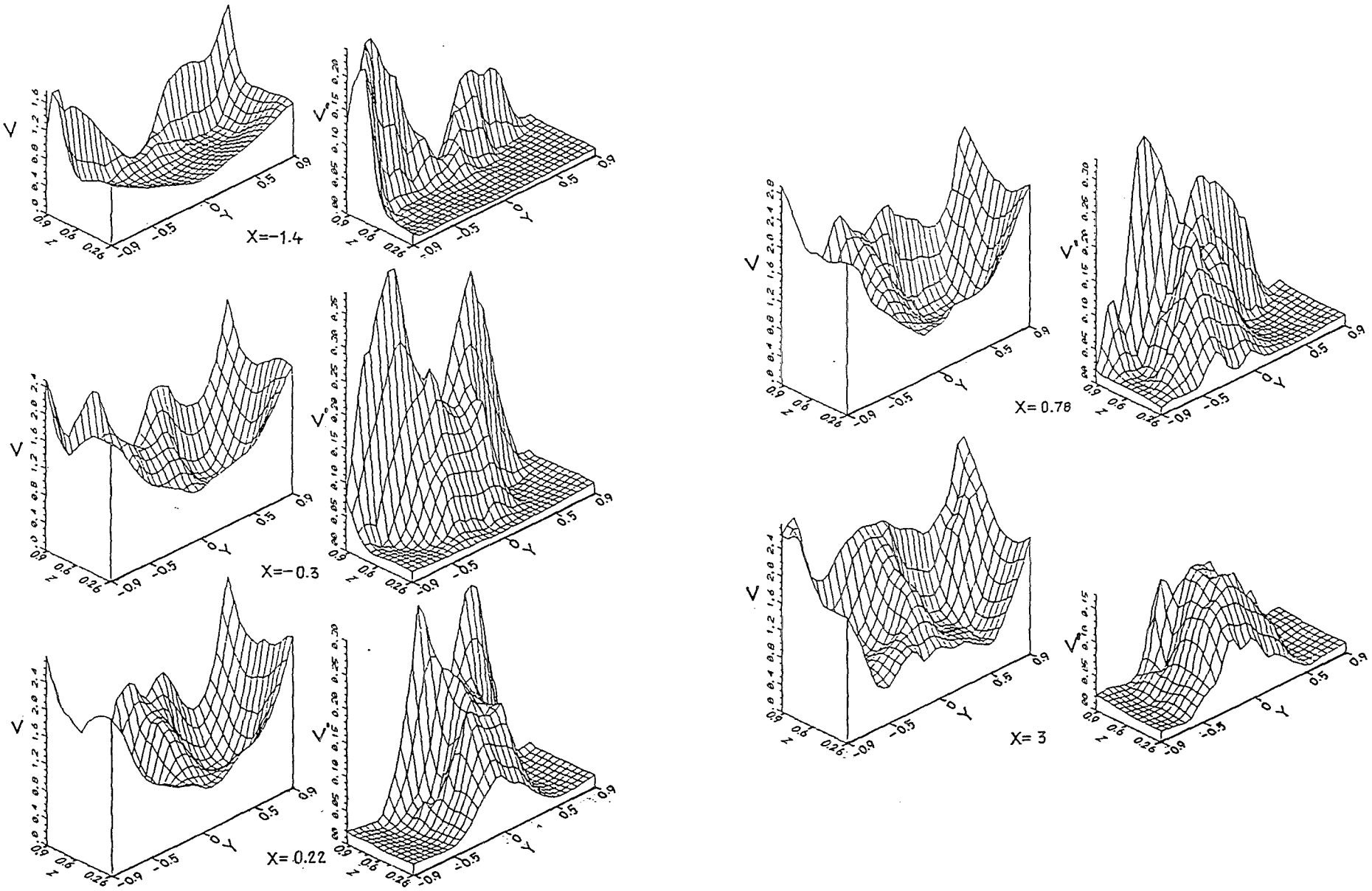

Fig. 4.8 Velocity and velocity fluctuations for C=0.122, Ha=230 and N=35, (hot wire parallel to z)

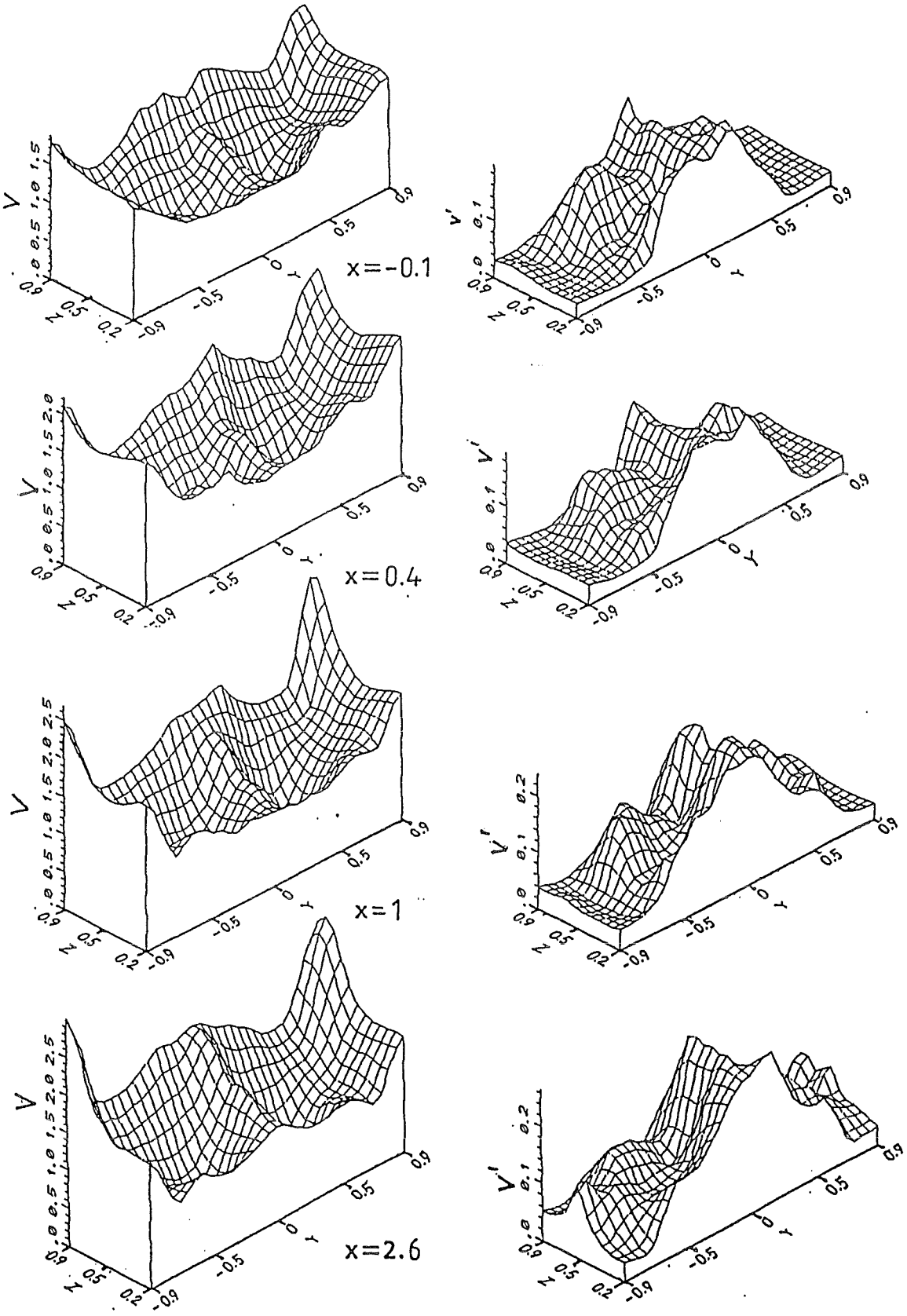

Fig. 4.9 Velocity and velocity fluctuations for C=0, Ha=255 and N=38 (hot wire parallel to z)

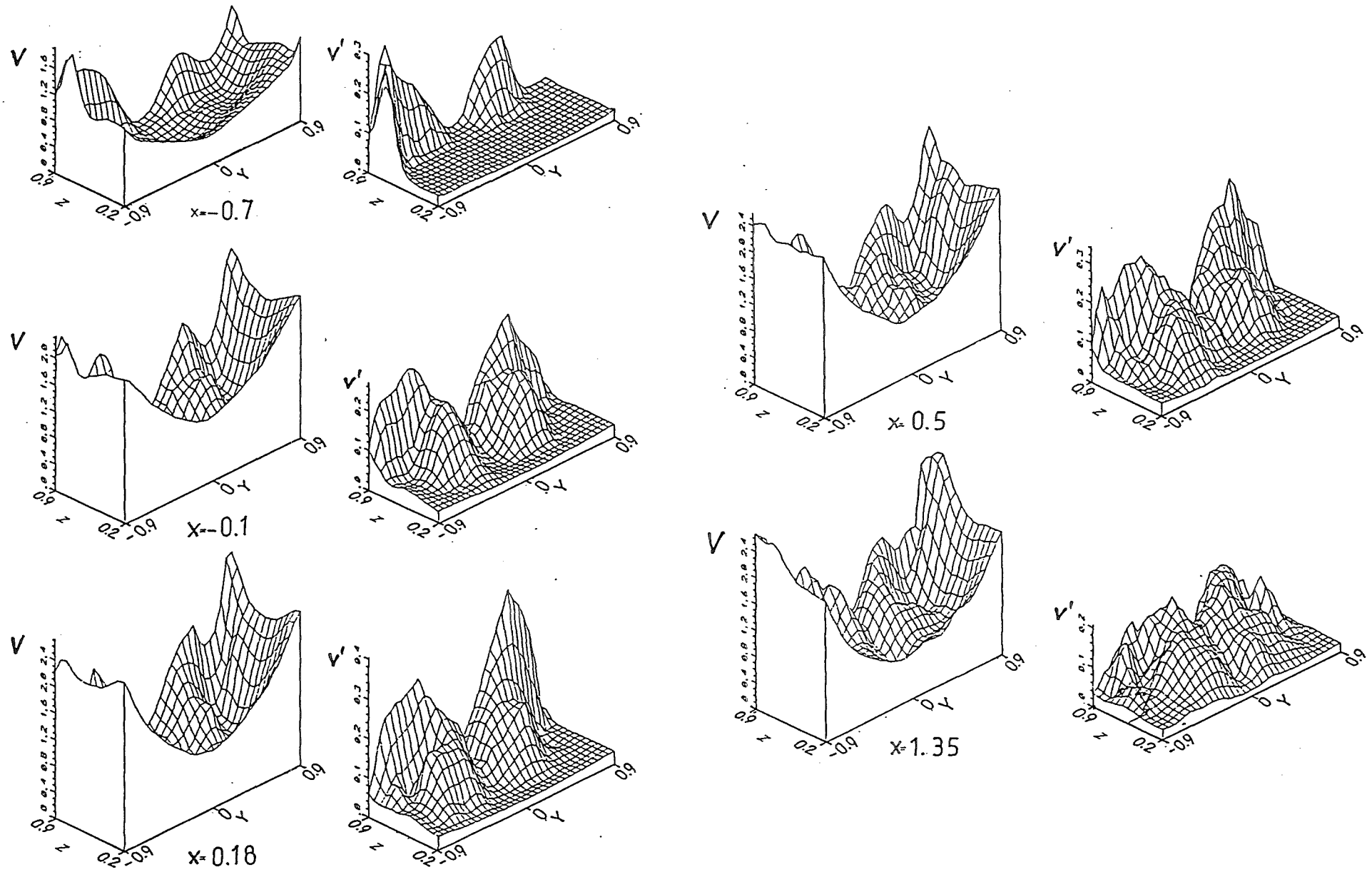

Fig. 4.10 Velocity and velocity fluctuations in the toroidal duct with a highly conducting First Wall for Ha=230 and N=35 (hot wire parallel to z)

Figure 4.9 shows the corresponding results for the bend with nonconducting walls, again there is no qualitative difference to the results with thin conducting walls.

Figure 4.10 contains results for the test section with a much better conducting FW. Again, it is clearly seen that the instabilities first occur in zones close to the FW. The thick FW seems to reduce the growth of the (supposed) vortices with increasing x, the minima of the mean velocity and velocity fluctuation at $y \approx 0$ could mean that the vortices, generated near the corners to the side walls, are still separated by a zone of nearly stagnant liquid.

Figure 4.11 finally shows a result from hot wire measurements where curves of

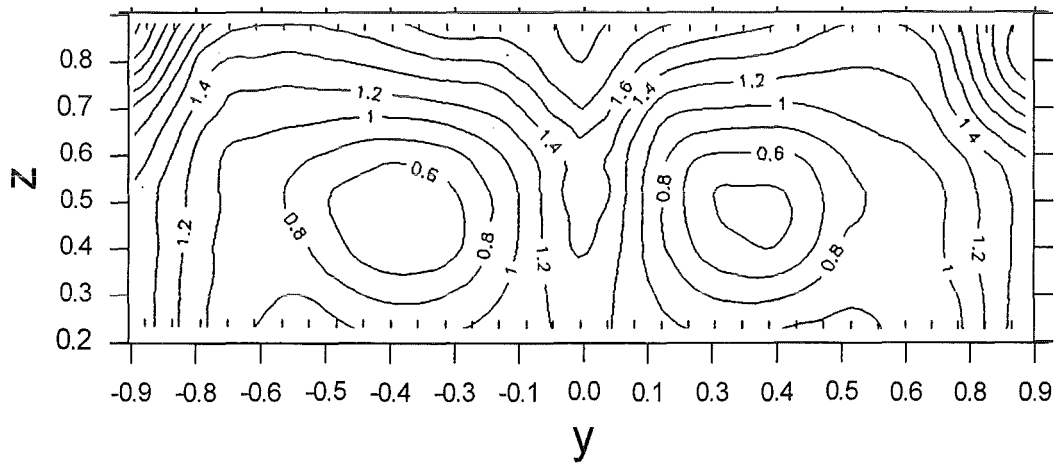

Fig. 4.11 Curves of constant velocities (from hot wire probe) in toroidal cross section (Ha = 255, N = 18, x = 2.7)

equal signal heights (equal velocities) are shown. Again this figure could be characteristic for jet type flow with only a velocity component in x direction or a flow in x direction with superimposed vortices.

4.1.3 Measurement of the Flow Structure in the Toroidal Duct with Potential Probes

In order to investigate in more detail the flow structure the triple potential probe (STP) was built (Fig. 2.7) which measures independently the velocity components v and w in the y,z-plane .

Figure 4.12 contains results for v and w and the velocity v_{xy} which is the vector sum of v and w. This figure shows very clearly the existence of a pair of vortices

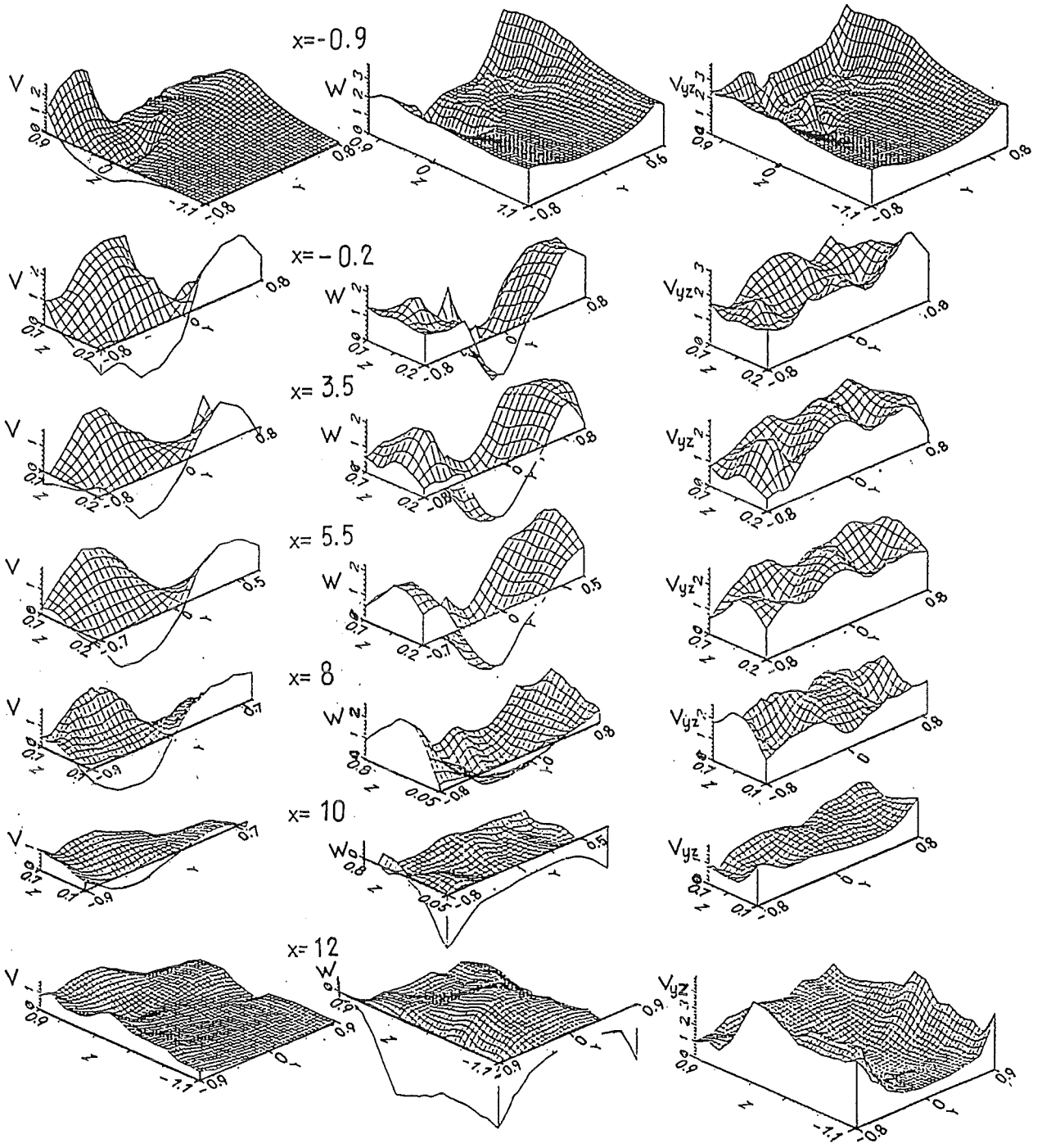

velocity component V velocity component W velocity V_{yz} perpendicular to x

Fig. 4.12 Velocity components perpendicular to x (potential probe) for C=0, Ha= 255 and N=38)

which rotate in opposite directions with a downward flow at $y \approx 0$. Furthermore it can be seen that the sense of rotation does not change up to the end of the toroidal duct. A remarkable damping of the vortex strength with increasing x is not observed. (The same results were obtained up to the maximum investigated value of N = 150). The change of the w distribution at x=4.2 is attributed to the influence of the downstream bend whose inner corner is positioned at 4.9. The position x=6.2 is already in the region of the outlet radial duct which explains the strongly changed velocity distribution.

The characteristic features of the observed vortices are in contradiction to the theoretical results valid for inertialess laminar flow which predicts an upward vortex flow at $y \approx 0$ in the first half of the toroidal duct and an increasing downward flow in the second half; compare Section 3. Therefore, it seems to be reasonable that these vortices are caused by an effect which is not taken into account in theory : inertia.

The following phenomenological description is proposed, see Fig. 4.13: The 3d

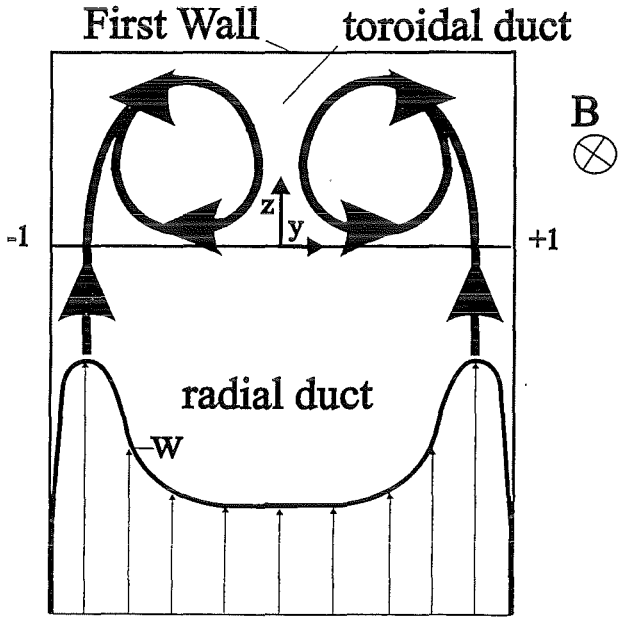

Fig. 4.13 Schematical graph of assumed mechanism for vortex generation

electric currents in the radial duct produce an increasing M-shaping when approaching the bend. This M-shaping causes an increased momentum flux ρw^2 in the side layers at $y = \pm 1$. While being deflected into the toroidal direction these layers approach the FW and are deflected there from both sides towards the middle of the FW (y=0) and flow downward.

This generation of vortices is quite different to pure hydrodynamic flow in bends where a vortex pair is caused by inertia effects, too. The sense of rotation, however, is opposite because the fluid momentum flux in the boundary layers at $y = \pm 1$ is lowest, compare e.g. /21/.

If the vortices are generated by inertial forces, then the vortex strength should decrease with increasing N. This tendency can be seen in Fig. 4.14 where velocity distributions for different N at three different positions z are shown. For a further increase of N, these vortices are expected to vanish and for very high N the flow pattern predicted by the CFA should establish. The value of N where this transition occurs is dependent on the wall conductivity and the Hartmann number as well. In detailed experiments /10/ with $C = 0.04$, $Ha \geq 500$ and $N \geq 1000$ a good agreement was obtained between the numerous potential wall probe measurements and the CFA results, indicating that vortices no longer existed.

The Figs. 4.15 and 4.16 contain characteristic examples of the time dependency of the hot wire signals. In Fig. 4.15 the signals for two different values $z = \text{const.}$ close to the FW are shown. The minimum of the fluctuations at $y \approx 0$ is quite expressed indicating that the vortices are still separated, see also Fig. 4.7. For smaller z the fluctuations become smaller and vanish in the zone close to the Second Wall.

Figure 4.16 shows corresponding results for $x = 1.6$ and a vertical traverse at $y \approx 0$. In this case the vortices have grown together and cover the total cross section. For all values of z, high fluctuating components are observed. (The signal noise level is about 1.5 mV). Both figures show characteristic frequencies in the range of some Hz. Such low frequencies for a cross-sectional velocity of 2.2 cm/s are quite characteristic for MHD instabilities as will be shown in more detail in Section 4.2.3.

4.1.4 Conclusions for Fusion Reactor Blankets

For the considered Pb-17Li blanket with the radial-toroidal U-bend (Fig. 1a) the Hartmann numbers and Interaction parameters ($Ha = 8000$, $N \approx 200$) are between the experimentally investigated values and the values assumed in the theoretical analyses (CFA). Therefore, the following extrapolations to blanket conditions are rather qualitative.

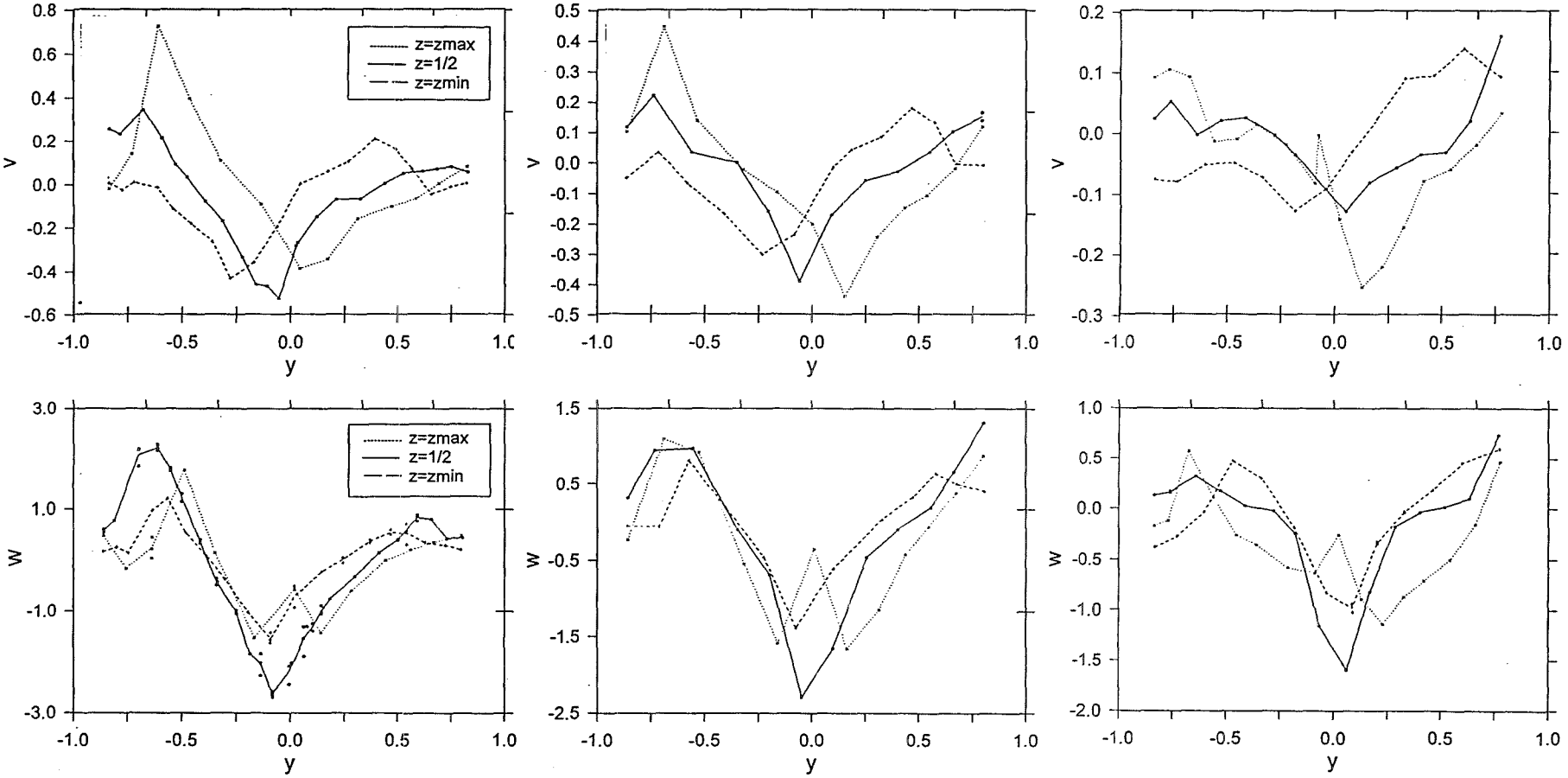

Fig. 4.14 Influence of N on vortex strength (x=6.9, Ha=255mm)

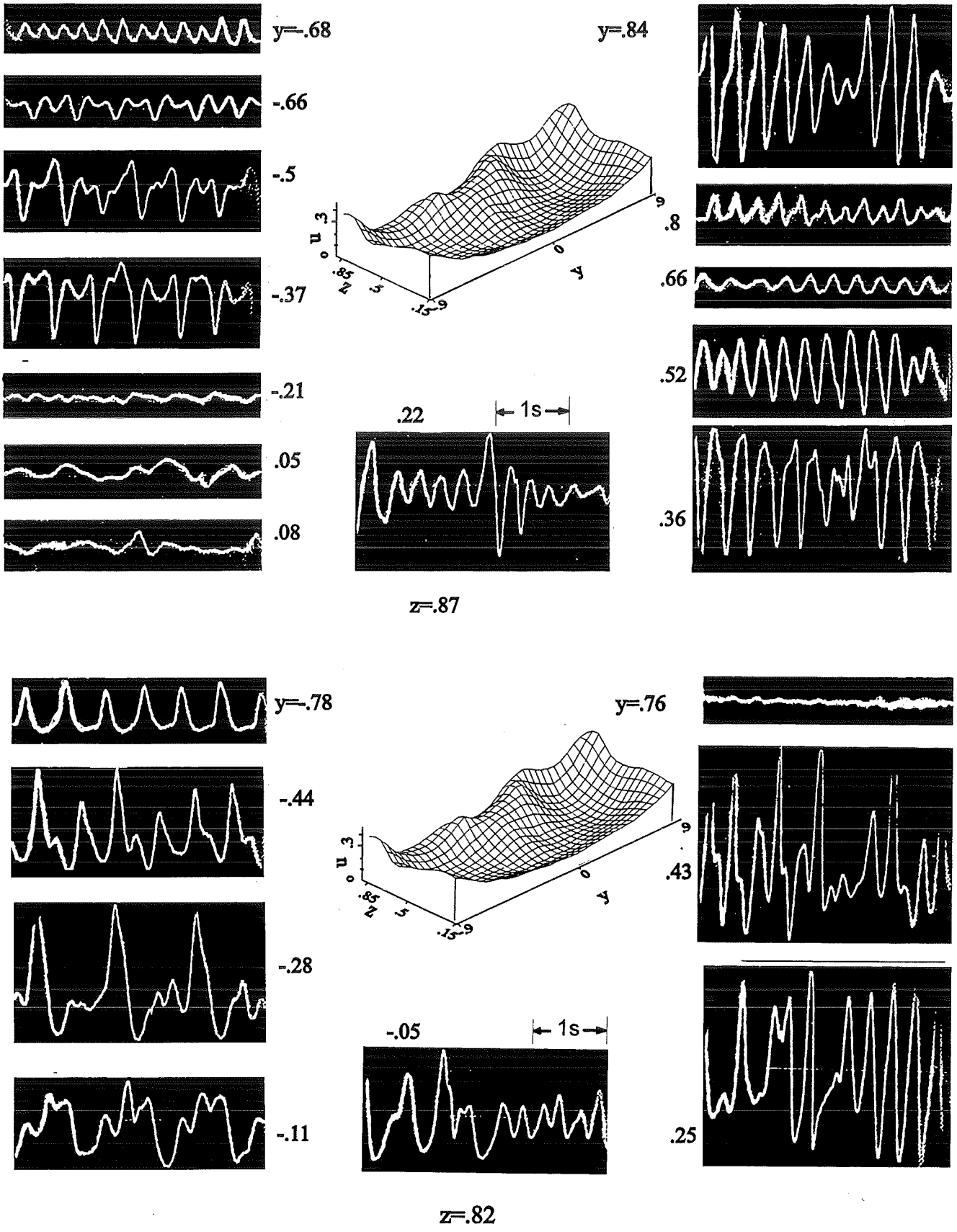

Fig. 4.15 Hot wire signals at x= -0.15 for C=0.122, Ha=230 and N=35

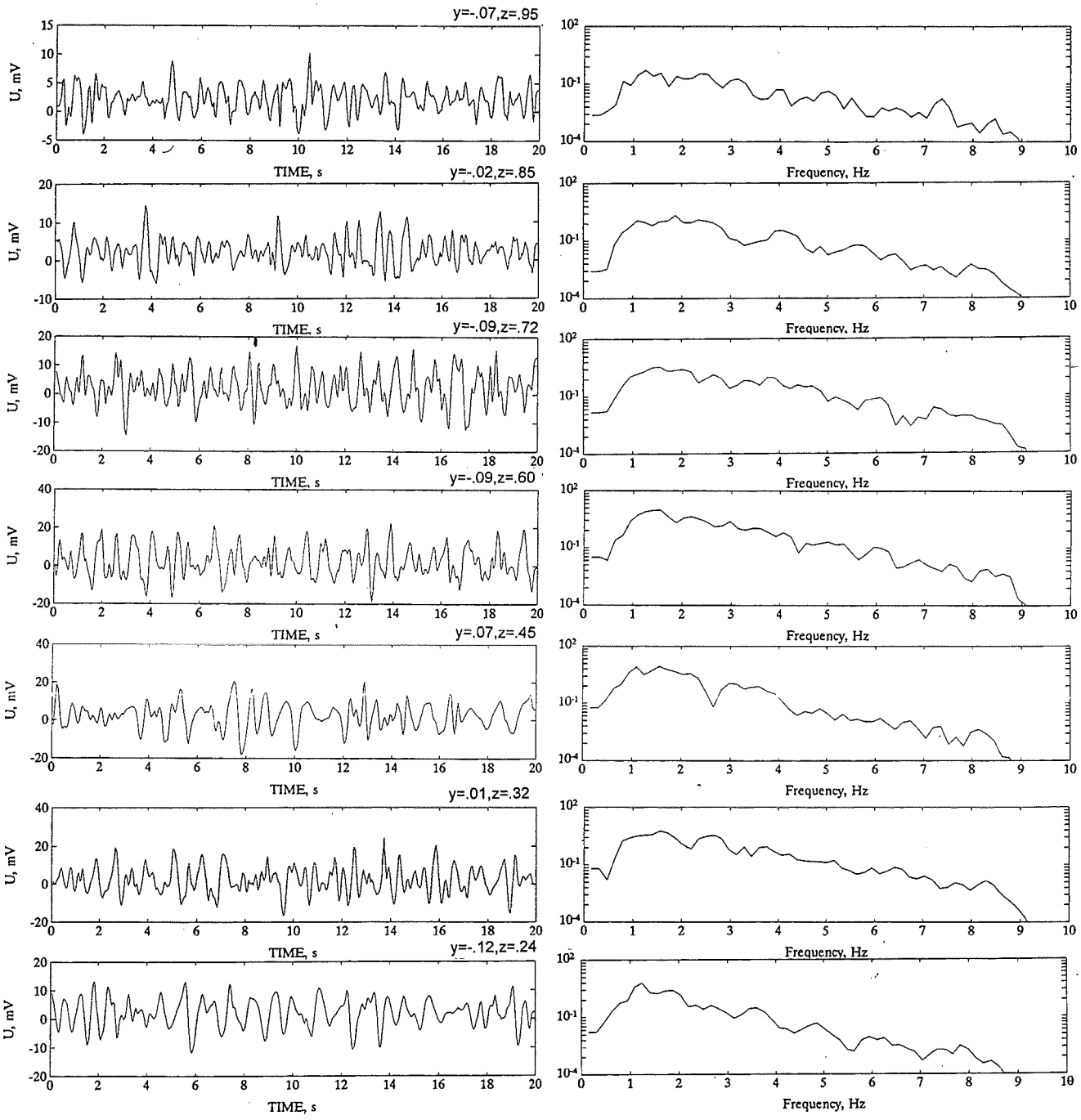

Fig. 4.16 Hot wire signals and spectra at x = 1.4 for C = 0.122, Ha = 230 and N = 35

It was observed experimentally, that with increasing N liquid is increasingly pushed to the FW as predicted by the CFA. Due to this fact the heat transfer from the FW should be much more favourable even for laminar flow than that resulting from a constant velocity profile with laminar flow as assumed in the design of the blanket according to Fig. 1a /1/.

The occurence of vortices with axis parallel to B is generally not accompanied by an expressed additional pressure drop as observed in duct flows already many years ago /5/. From different bend experiments /10, 11/ with one duct parallel to B the following pressure drop correlation was deduced

$$\Delta p = K_1 + K_2 N^{-1/3} + K_3 Ha^{-1/2},$$

where the coefficients K_i depend on the flow bend and wall conductance ratio. Using the results from a similar U-bend geometry /10/ as investigated in the present experiments only a pressure drop increase of less than 10% is obtained by changing the Interaction parameter from N = 1000 (no vortices in /10/) to N = 150 (vortices in present experiments).

If the vortices exist, they would be very beneficial for heat transfer. The transversal velocities should provide a very effective temperature equilibration in the FW duct. Larger channels with lower mean velocities could be used which could result in considerably simplified designs. The present knowledge, however, is not sufficient to judge if these vortices occur at blanket relevant conditions. If such vortices would not be generated there is still the possibility to provoke the vortex generation in the bend zone by MHD relevant measures (e.g. shaping of the flow distribution by mechanical inserts or locally differing wall conductivities). Due to the small damping of vortices with axis parallel to B, such vortices could exist over a considerable flow length.

4.2 Bend Perpendicular to B (bpeB-exp)

The strong 3d electric currents which gave rise to a strong increase of the velocities near the side walls $y = \pm 1$ in the previous experiments, do not occur in the present flow geometry as outlined in Section 3. According to the CFA, the velocity distribution in the core for high values of Ha and N is similar to potential flow for both conducting and nonconducting walls. A distinct difference between con-

ducting and nonconducting walls is the occurence of M-shaping at the side walls for $C>0$. This difference has a strong impact on the flow structure as will be demonstrated later. Therefore, the results for the two wall conductance conditions are presented separately.

Of special interest in these investigations is the question if the 90° bend acts again as a promotor of instabilities. If instabilities with axis parallel to B are again favoured, then the inner corner could play a special role as a turbulence promoter.

Compared to the previous experiments, the maximum achievable values of Ha and N have about doubled because the characteristic length in direction of B has changed. (Besides the magnetic field strength B could be increased to $\approx$ 1.2 Tesla by narrowing the magnet pole shoes).

4.2.1 Velocity Distribution in the Bend with Nonconducting Walls

In this section results obtained with the STP are reported. Measurements in the inlet duct at $z = -3.2$ showed again that the velocity distribution was very homogeneous and the turbulence level was less than 4 % (which proved that the combination of honeycomb and copper bars worked as anticipated).

Figure 4.17 shows velocity distributions in the downstream duct of the sharp-edged bend for $y=0$ and different values of Ha and N. For the lowest values the velocity distribution should be similar to that for pure hydrodynamic flow. In fact, the velocity distribution is very similar to that for $Ha=N=0$ shown in Fig. 4.5: a strong separation zone exists downstream of the inner corner. In contrast to the previous results this separation zone persists up to significantly higher values of N; only at $N\approx 200$ the zone of reduced velocities is limited to a small zone downstream of the inner corner. The reason for the larger separation zone are the missing 3d currents which otherwise dominate inertial forces already at moderate values of Ha and N. The theoretical analyses based on inertialess flow (see Fig. 3.3) are therefore not well suited to predict the flow distribution in the downstream zone close to the inner corner.

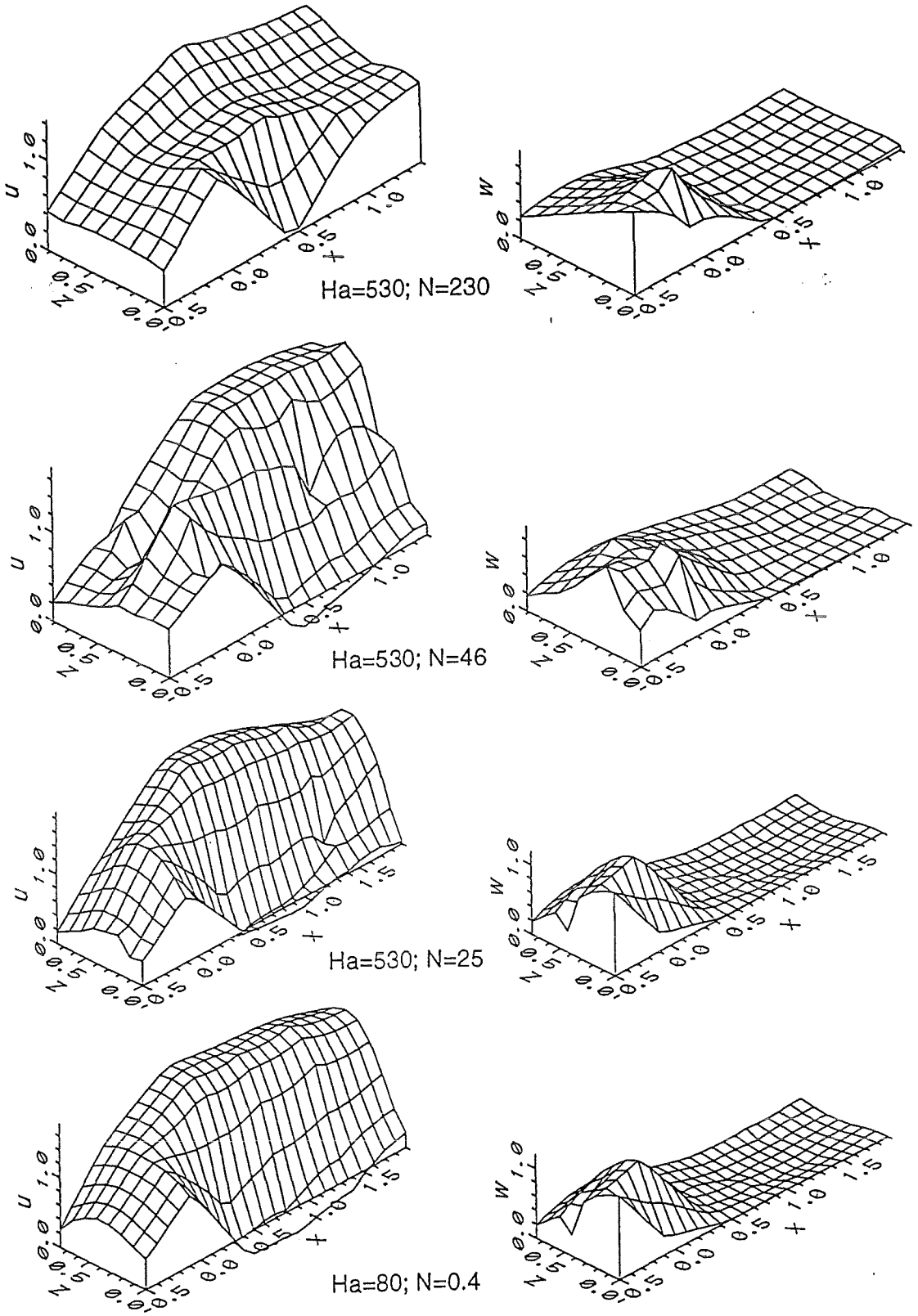

Fig. 4.17 Mean velocity distributions in downstream duct of nonconducting sharp-edged bend for duct midplane (y = 0)

Figure 4.18 contains corresponding results for a position y = -0.8. The velocity distributions are very similar to those in the duct midplane which means the distributions are fairly two-dimensional (2d), depending only on x and z. Therefore, in the following only results with the STP at y=0 are presented. More details on the 2d structure will be given in Section 4.2.2.

The next figures show distributions of the mean velocities u and w and the corresponding mean values of the velocity fluctuations u′ and v′. For completeness the distribution of the correlation coefficient K is also shown which is the product of the instantaneous fluctuating components normalized by their mean values (for details, see Appendix I). The distributions of the coefficient K might be of interest for detailed analyses of the structure of the flow instabilities; in this report, K is not further analyzed.

Results for N=8 at different position x are presented in Fig. 4.19. The position x=0.25 is very close to the inner corner. The influence of flow separation caused by this corner should be restricted to small values of z. It is seen that for x=0.25 the turbulence level in the upper part of the cross section is significantly increased compared to the value in the inlet duct. This might be caused by the strong velocity gradients in this region or by a marked recirculation zone near the outer corner. With increasing x the fluctuations increase significantly in the lower half of the duct cross section where flow separation and eventually flow recirculation exist.

For large N (Fig. 4.20), the increase of the turbulence level in the upper duct portion is not observed for x=0.25, however, an increased turbulence level exists in the total cross section. For increasing x, the fluctuations close to the upper sidewall are damped. In the lower duct part the fluctuations first increase with increasing x in the zone of strong velocity gradients and decrease when the velocity profile flattens.

Measurements with a similar test matrix were performed with a rounded bend. For this geometry smaller inertia effects are expected resulting in a reduced separation zone. Figure 4.21 shows results for a cross-section close to the inner bend corner. For an Interaction parameter close to zero the mean velocity exhibits a potential type behavior. The turbulence level is very small. For the higher N

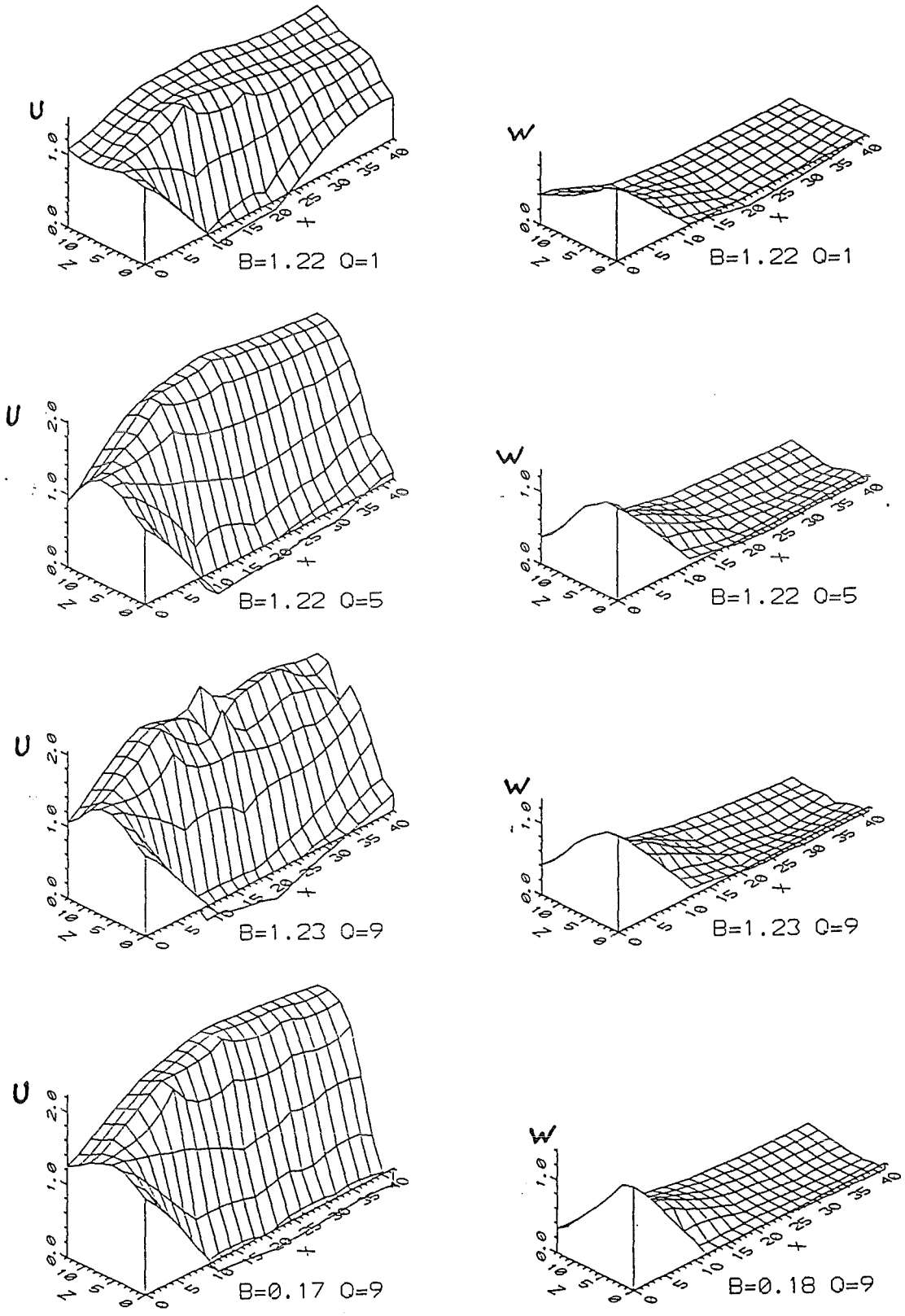

Fig. 4.18 Mean velocity distributions in downstream duct of nonconducting sharp-edged bend for y = - 0.8

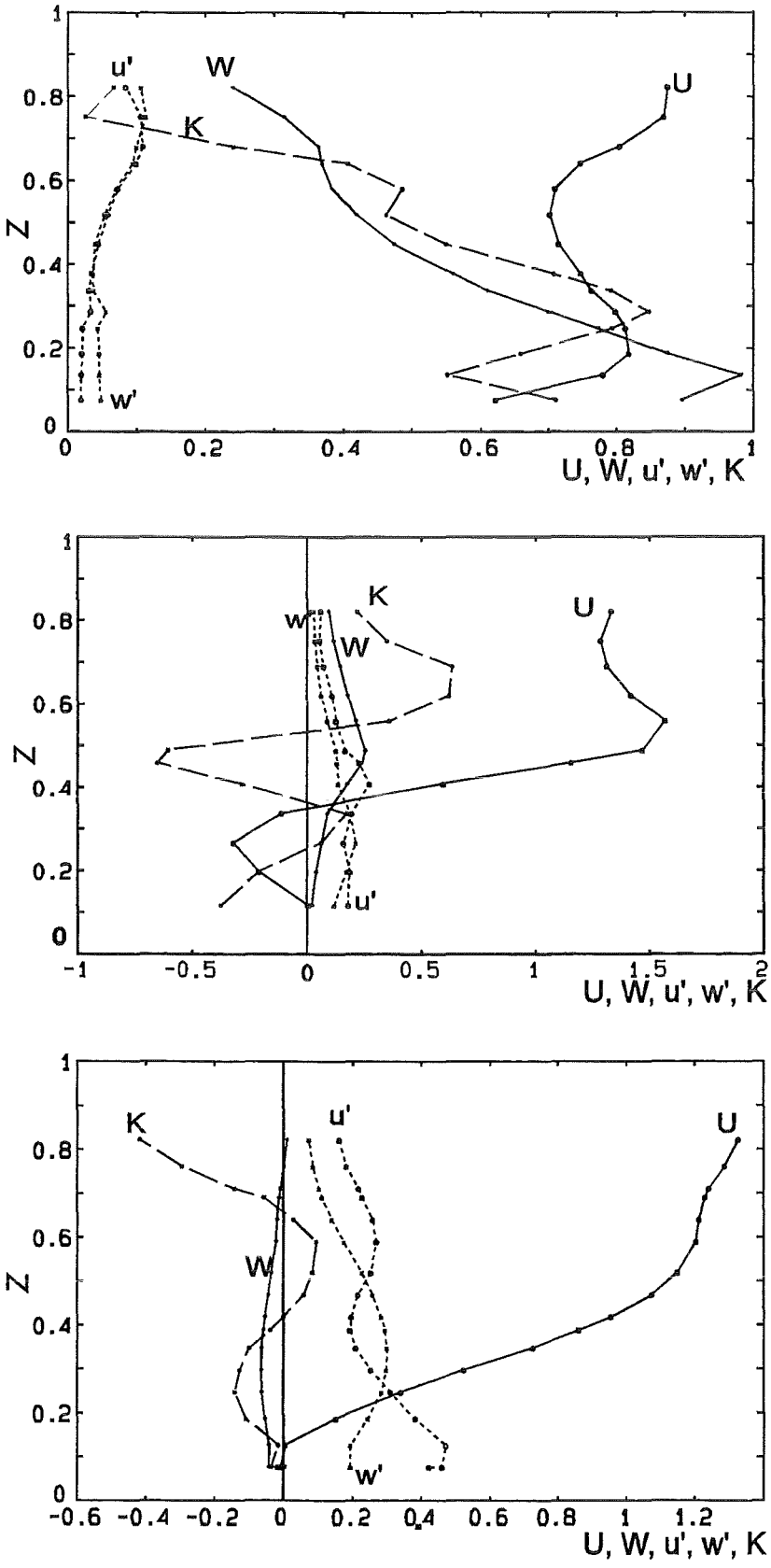

Fig. 4.19 Velocity and velocities fluctuations in sharp-edged nonconducting bend (C=0; N=8, Ha=530; STP)

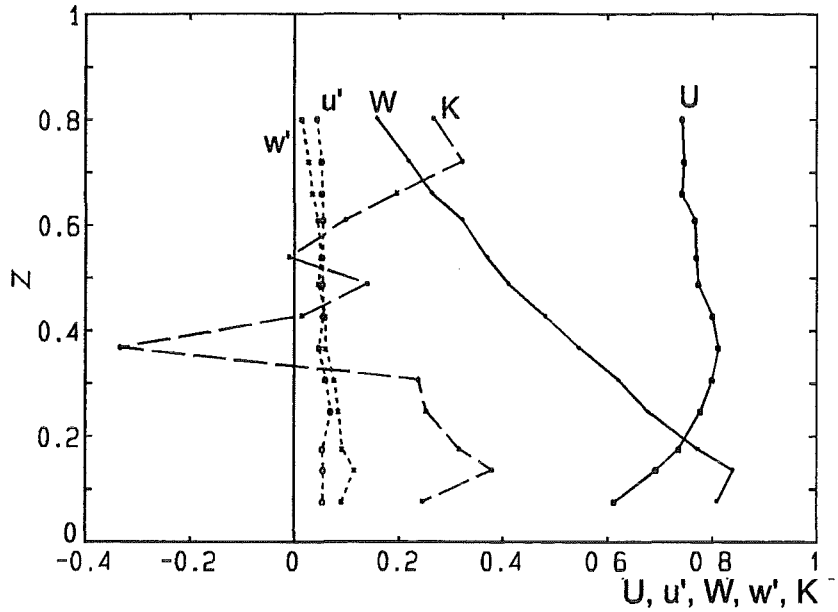

X=0.25

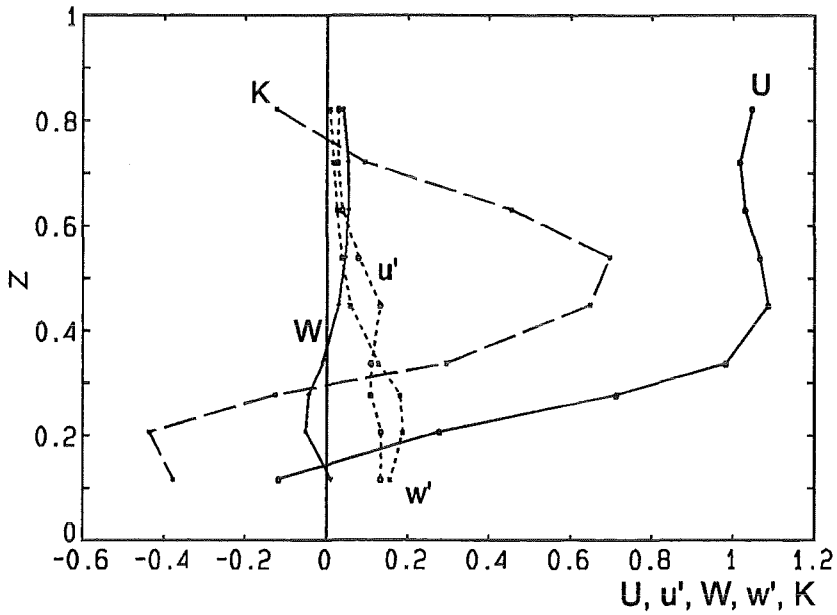

X=1.02

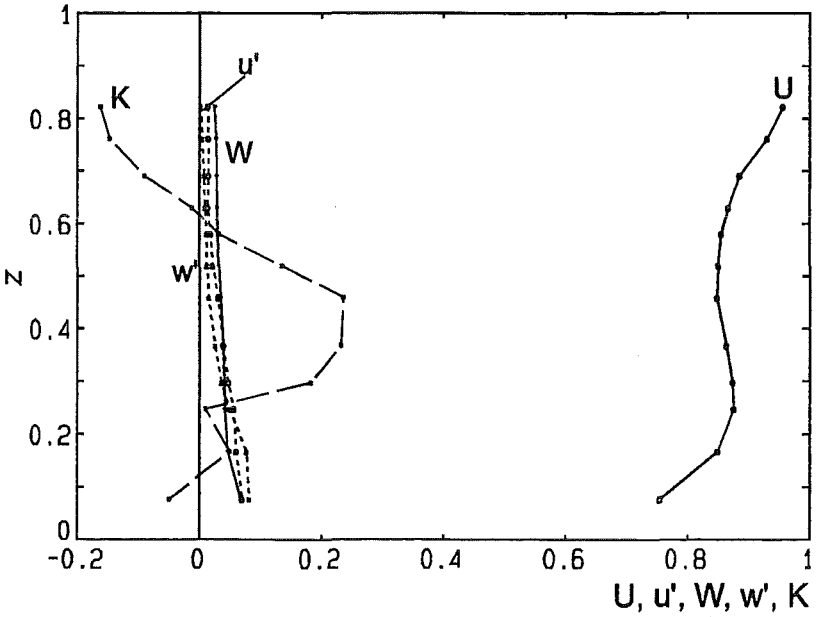

X=2.53

Fig. 4.20 Velocity and velocity fluctuations in sharp-edged nonconducting bend (C=0; N=150; Ha=530; STP).

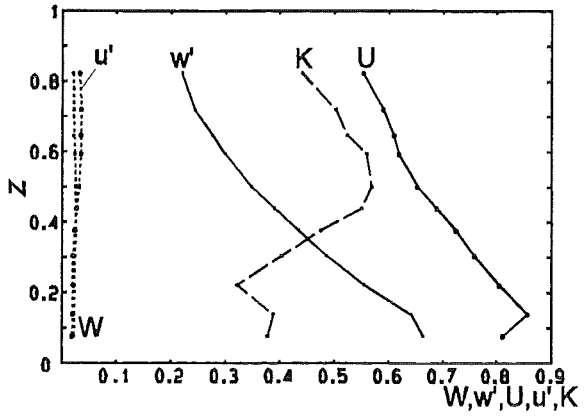

N = 0.04

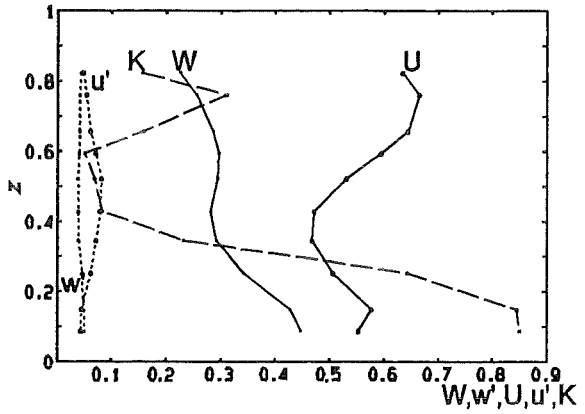

N = 8

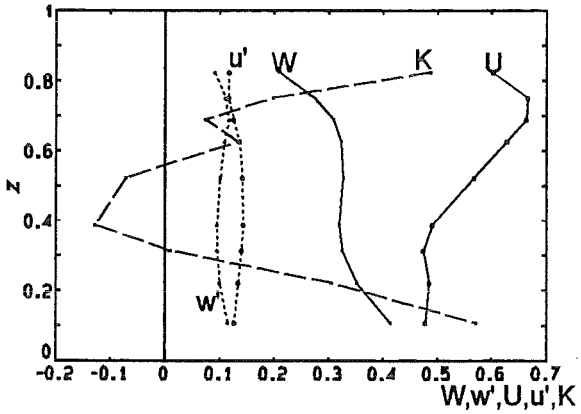

N = 32

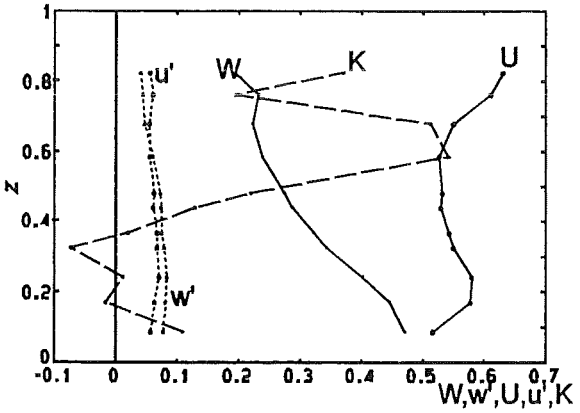

N = 91

Fig. 4.21 Velocity and velocity fluctuations in rounded nonconducting bend (C=0; x=0.25; Ha=530; STP)

the mean velocity profiles are changed and the turbulence levels have increased in the total cross section.

Comparing the results for the sharp-edged and rounded bend for $x=0.25$ and large N one can observe that in both cases the turbulence level has increased compared to the value in the test section inlet (and compared to the turbulence level for ordinary hydrodynamic flow at $x=0.25$). The conclusion, therefore, is that in the bend itself (and not only downstream of the bend in the separation zone) mechanisms exist which promote turbulence.

The dependence of the flow structure on the flow path x is shown in Fig. 4.22 for $N\approx 8$. The separation zone near the lower sidewall is smaller than for the sharp-edged bend, compare Fig. 4.19, however, the values of the turbulence level differ not significantly.

4.2.2 Velocity Distribution in the Sharp-edged Bend with Conducting Walls

For the bend with conducting duct walls strong 2d electric currents exist in the core which generate Lorentz forces which partly counteract with inertial forces. Of special interest is, if instabilities are generated near the side walls due to the characteristic M-shaping.

The Figs. 4.23-4.25 contain results for $C=1.0$ obtained with a TSP or a STP. For $C=1.0$, the accuracy of velocity evaluation is no longer satisfactory, as mentioned in Section 2.2.2. Sensitivity calculations with the CFA showed that the assumption of negligible currents resulted in velocities which could be about 30 % of the correct value. Therefore, these measurements are rather qualitative, however, essential tendencies should be reproduced.

Figure 4.23 contains results for different N in the entrance zone of the downstream duct ($x=0.25$) obtained with the TSP. The mean and fluctuating velocity components u_i and u'_i at $y=0$; 0.4 and 0.8 are shown. Additionally the distributions of the correlation coefficients $K'_{12}, K'_{23}, K'_{13}$ are presented which are the products of the corresponding instantaneous fluctuating components normalized with the product of their mean values (for denotation see Appendix I). For $N=2.3$ the distributions are similar to those of ordinary turbulent flow. Inertial forces cause a distinct zone of flow recirculation near the lower sidewall. The turbulence level is about 4 % in the total cross section and the values of the correlation coef-

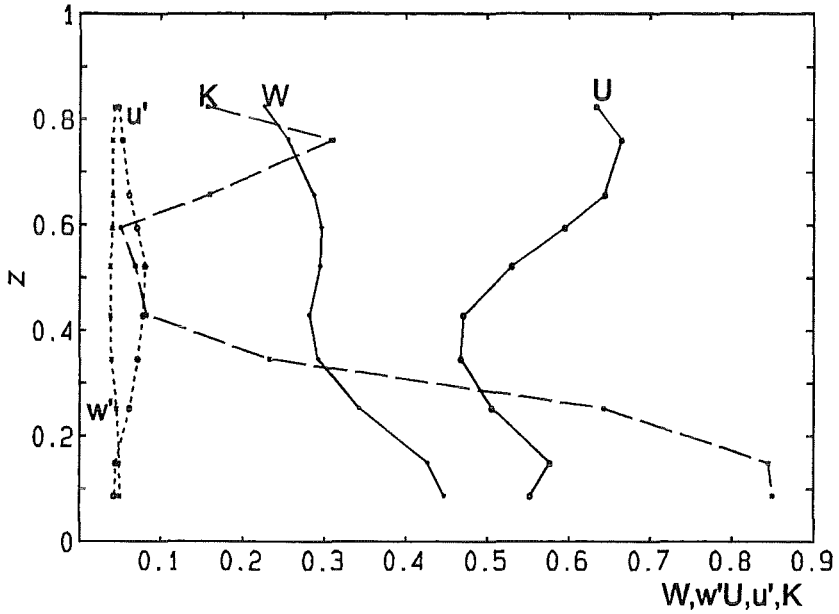

X=0.25

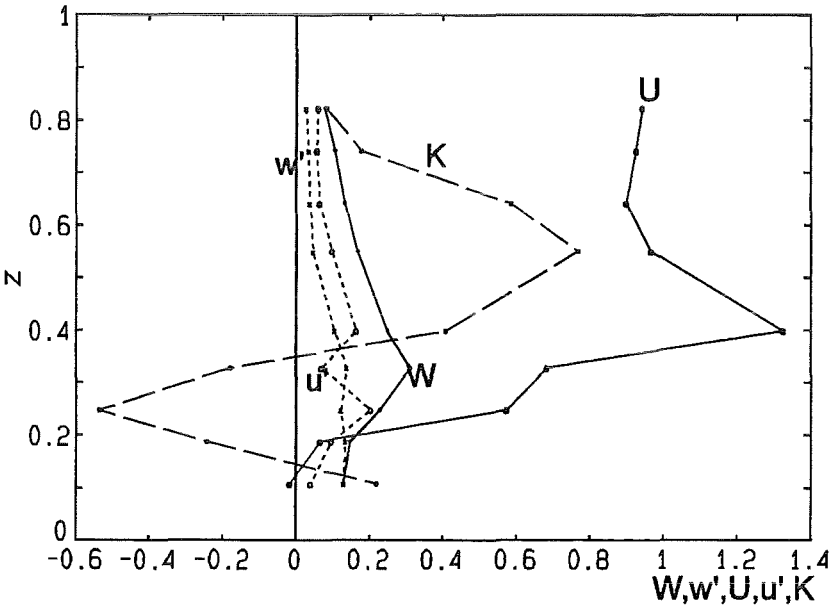

X=1.02

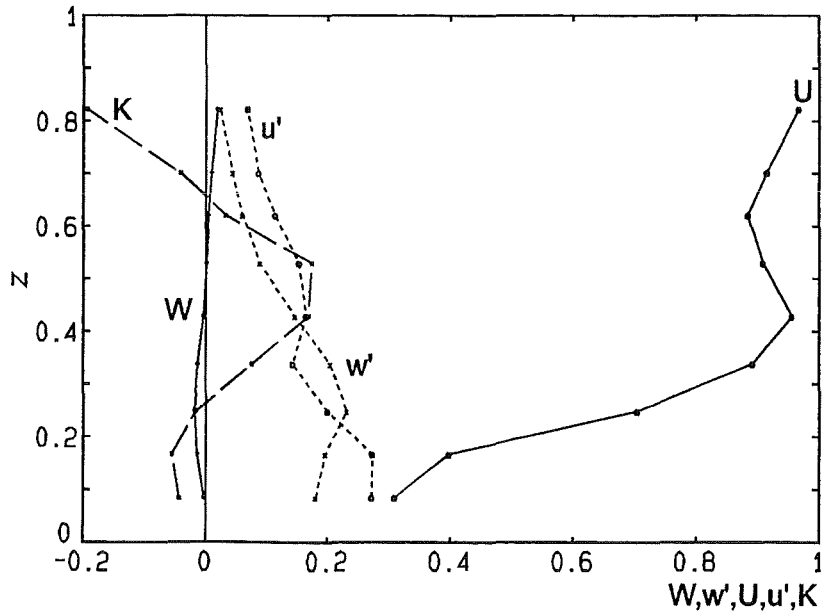

X=2.53

Fig.4.22 Velocity and velocity fluctuations in rounded nonconducting bend (C=0; N=8; Ha=530; STP)

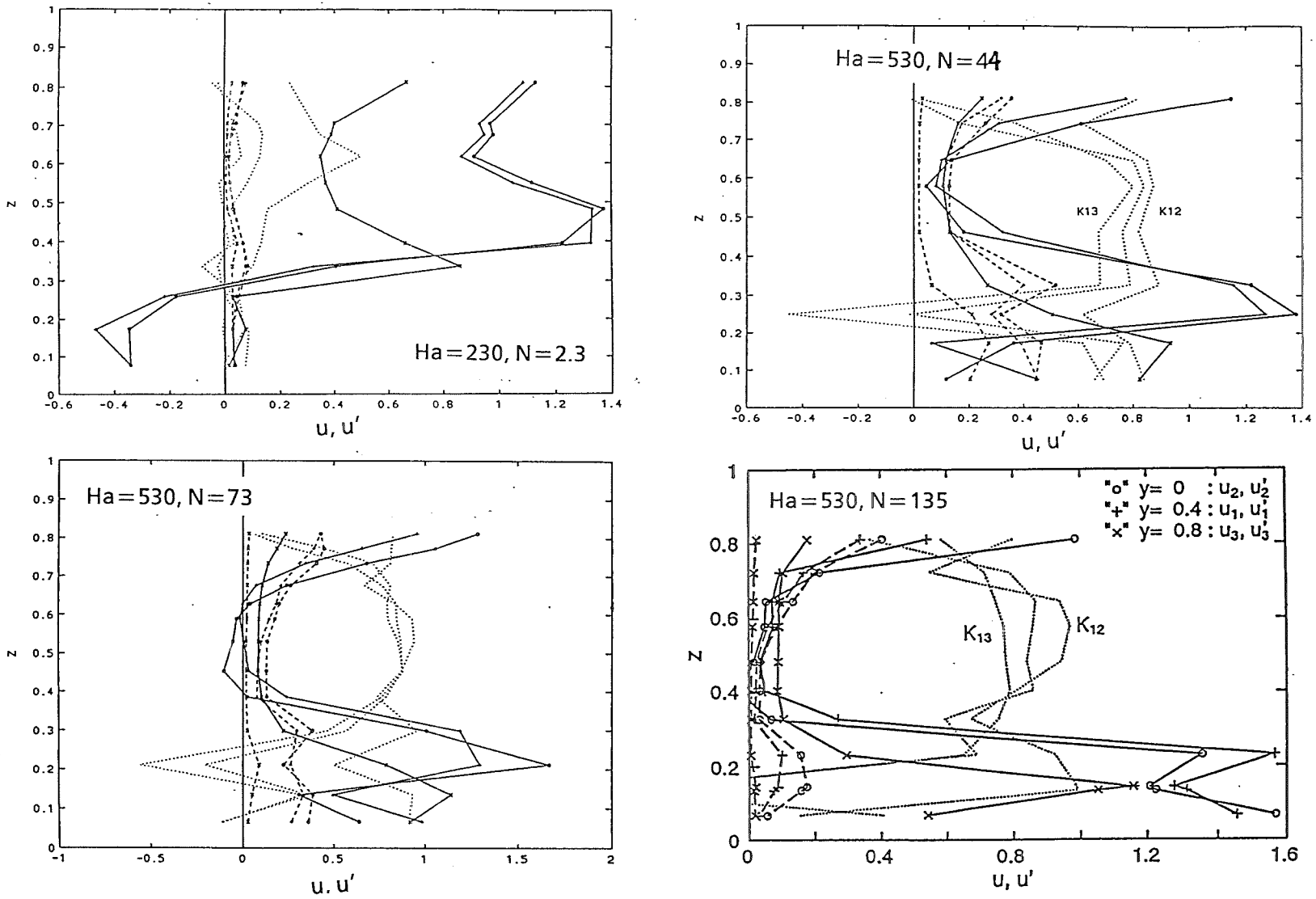

Fig. 4.23 Velocity and velocity fluctuations in sharp edged conducting bend (C=1.0; x=0.25; TSP)

ficients are quite small. For $N \approx 40$, the flow distribution has changed considerably: High velocities in the side layers occur (according to the predictions of the CFA, see Fig. 3.4). At the inner side wall this layer detaches from the wall downstream of the inner corner. With increasing N the high velocity jets become thinner and shift towards the sidewalls.

Due to the strong flow redistribution in the side layers during the deflection in the bend very high turbulence levels are measured in these zones with the probe positioned at $y=0$ and $y=0.4$. The probe at $y=0.8$ which is closest to a Hartmann wall measures much lower levels.

The development of these distributions with increasing flow path is shown in Fig. 4.24 for $N \approx 140$. Close to the FW, the mean velocity distribution does not change remarkably. The turbulence level, however, decreases with increasing x and becomes very small at $x = 4.5$.

At the lower sidewall MHD forces push the high velocity jet towards the wall and the recirculation zone disappears after a considerably shorter flow length than for the nonconducting duct. The turbulence level in the lower part of the cross section first increases with increasing x and after attachment of the separated side layer starts to decrease. At $x=4.7$ the level is still $\approx 15\%$, a value significantly larger than in the inlet duct.

Fig. 4.25 shows the influence of N for the axial position $x=2.5$ measured by the TSP. (Good agreements were obtained between STP and TSP measurements, compare e.g. the results for $N \approx 140$ and $x=2.5$ in Figs. 4.23 and 4.24). For $N \approx 140$, the side layers are the thinnest and a fairly constant core velocity has developed. The thickening of the side layers with decreasing N might be caused by inertia effects in the entrance region and the increased turbulence level which reduces velocity gradients.

Of special interest for fusion reactor blankets is the velocity and turbulence level distribution close to the FW ($z=1$). The TSP measurements for z_{max} showed a strong dependence on y. A parabolic type distribution (predicted by the CFA, see Fig. 3.2) is not always obtained because small errors in the probe adjustment may cause large measurement errors in zones with high velocity gradients. (In Fig. 4.23, the expected distribution is found except for the measurements at $x=1.5$ and $x=2.5$ which were performed after a new probe installation). An important

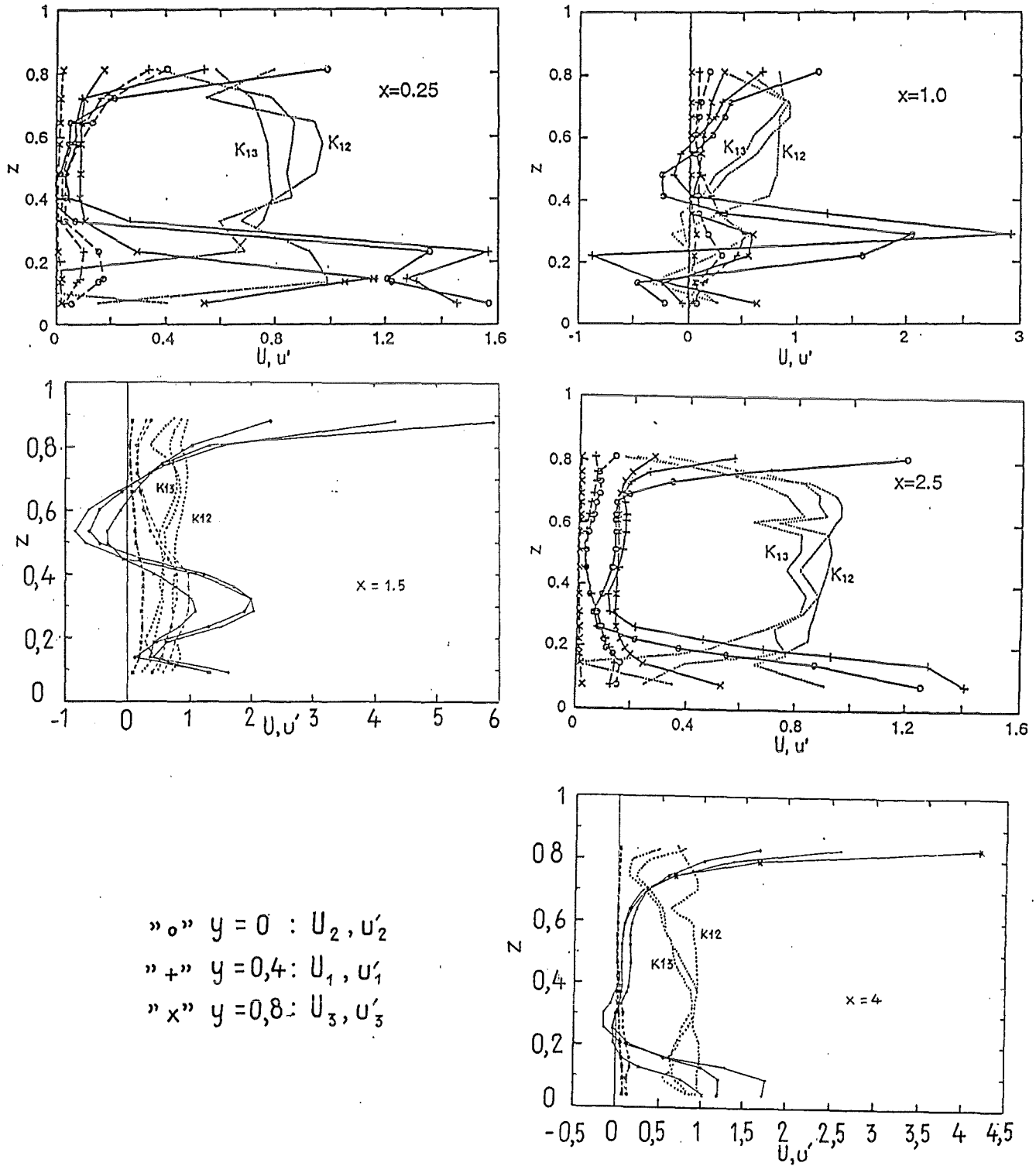

„o" y = 0 : U_2 , u'_2

„+" y = 0,4: U_1 , u'_1

„x" y = 0,8: U_3 , u'_3

Fig. 4.24 Velocity and velocity fluctuations in sharp-edged conducting bend (C = 1.0; N ≈ 140, Ha ≈ 530)

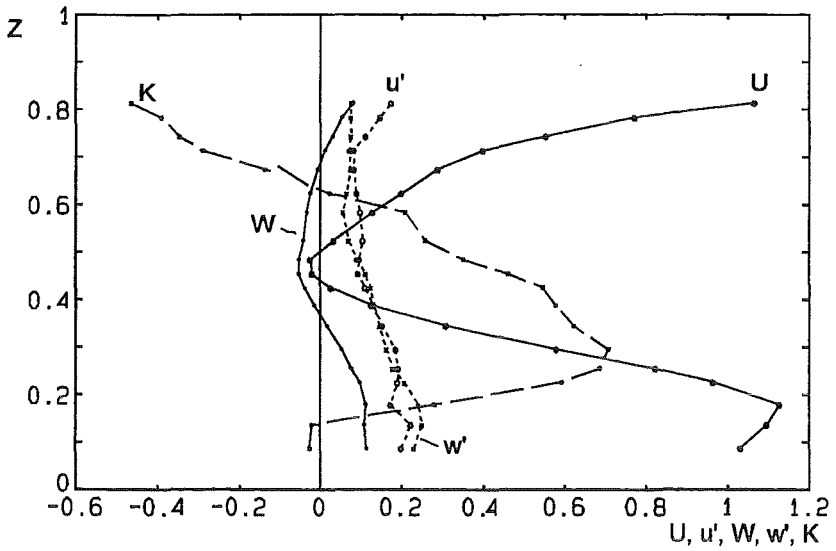

N = 35

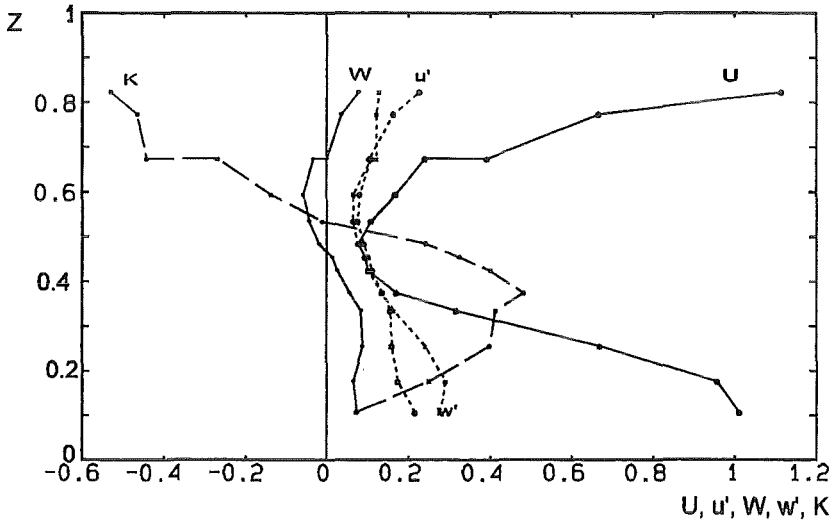

N = 67

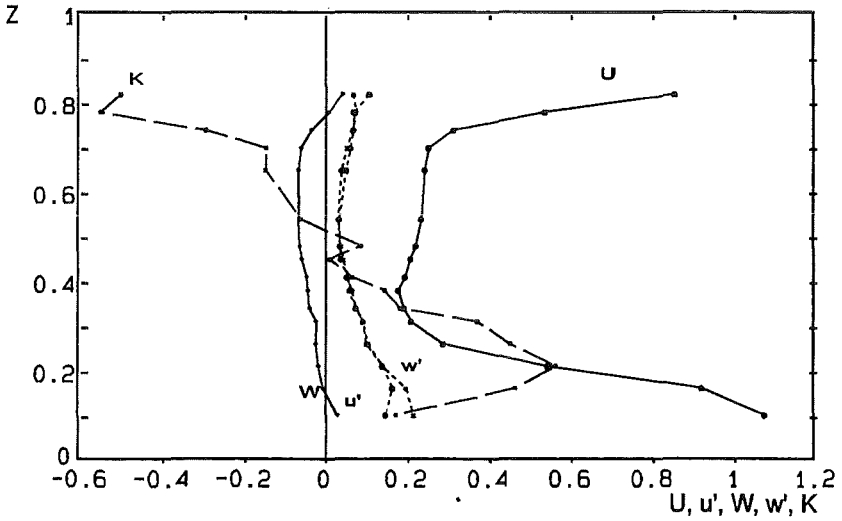

N = 139

Fig. 4.25 Velocity and velocity fluctuations in sharp-edged conducting bend (C = 1.0; x = 2.5; STP)

result is that the probe which is positioned closed to the Hartmann wall (y= -0.8) measures always a very low turbulence level. This low value in combination with the low mean velocity in the zone close to $y=\pm 1$ and $z = 1$ could result in unfavourable heat transport characteristics (hot spots).

In order to investigate in more detail the velocity distribution close to the FW some special experiments were performed using the specially built STP which could be traversed very close to the walls, see Fig. 2.7. In order to be more blanket relevant, a wall conductivity ratio of $C=0.1$ was used. This value results in a better accuracy of the measured core flow velocities compared to $C=1.0$, see Section 2.2.2. These measurements concentrated on one half of the upper part of the cross section (Fig. 4.26). For $N=8$, the dependency of the velocity distribution on the coordinate y is not very expressed compared to $N\approx 100$. For the high value of N, a considerable amount of the fluid is transported in the sidelayer. Again the thickness of the sidelayer is larger than predicted by the CFA. The decrease of the velocity with increasing y close to the FW is also smaller than predicted for laminar flow, both tendencies are propably caused by the increased turbulence level. Although the fluctuations become small for $y\rightarrow 1$, the quite large velocity in this zone will probably ensure a sufficient heat transport.

4.2.3 Analyses of Instabilities

The two-dimensionality of the time averaged velocity distribution for the bend with nonconducting walls was demonstrated in the Figs. 4.17 and 4.18. For the bends with conducting walls the previous figures also showed this two-dimensionality except for the side wall layers.

Of interest is if this two-dimensionality is also characteristic for the velocity fluctuations. The previous figures with the TSP results for $C=1.0$ show that the correlation coefficicents K_{12}, K_{23} and K_{13} increase with increasing N and reach high values in the largest part of the cross-section, indicating that the instabilities are fairly 2d, too.

For the nonconducting bend experiments the STP was mainly used (showing only that the u' and w' components are fairly equal at each measurement position). In order to investigate the two-dimensionality in a similar way as for $C=1$, additional test series were performed with the TSP positioned at $z\approx 0.5$ and the dependence of the correlation coefficients on N was determined for different axial

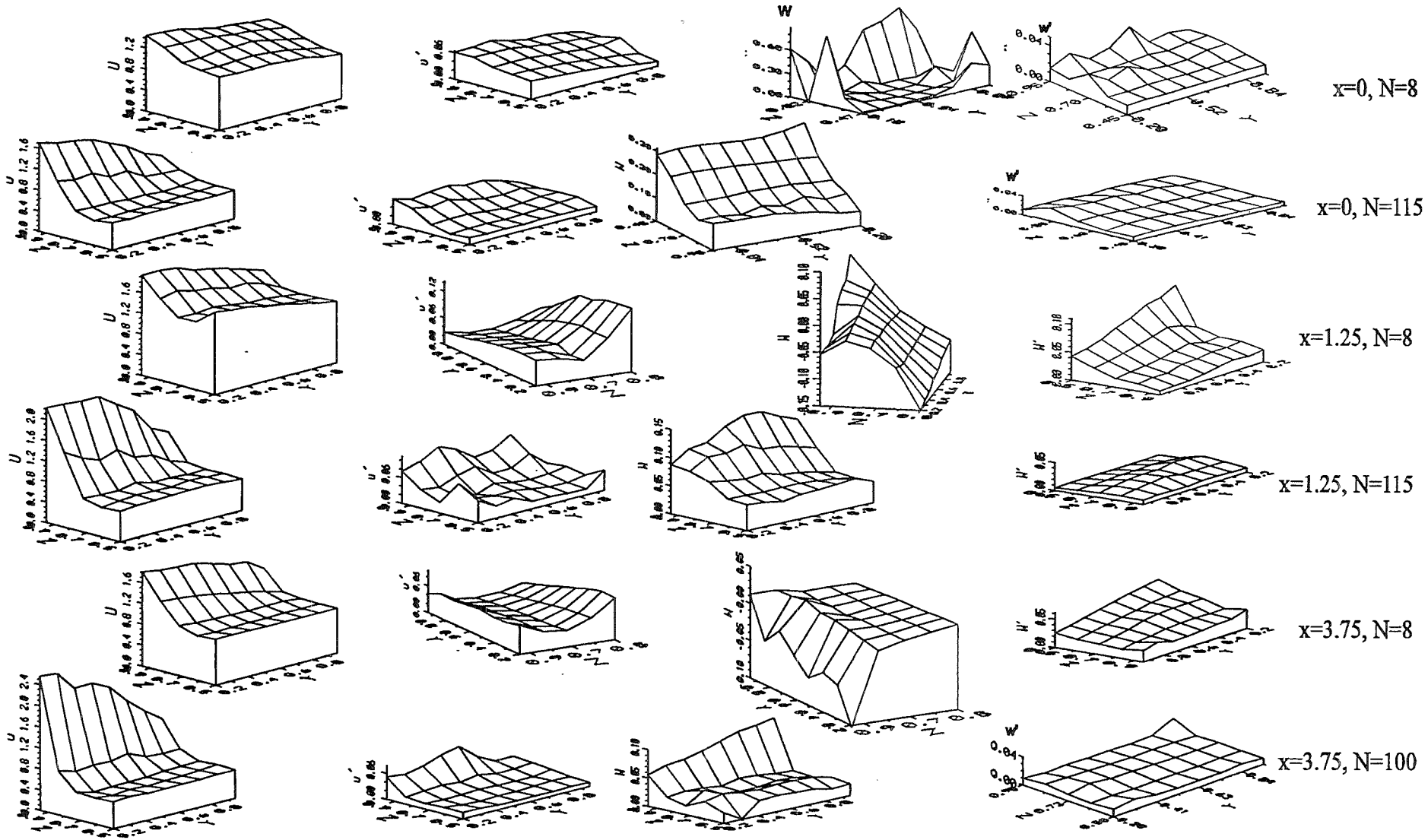

Fig. 4.26 Velocity and velocity fluctuations in sharp edged conducting bend (C=0.1; Ha=500; TSP).

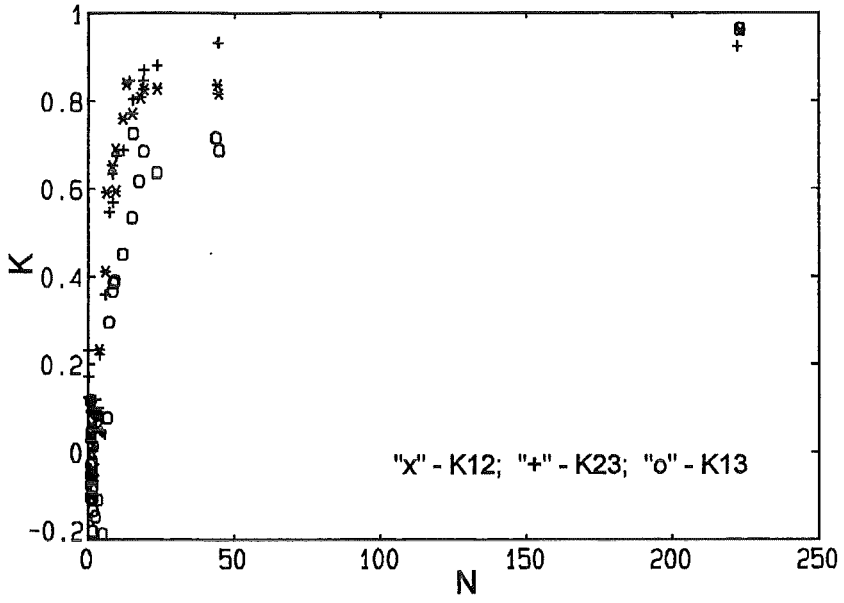

X=1.5

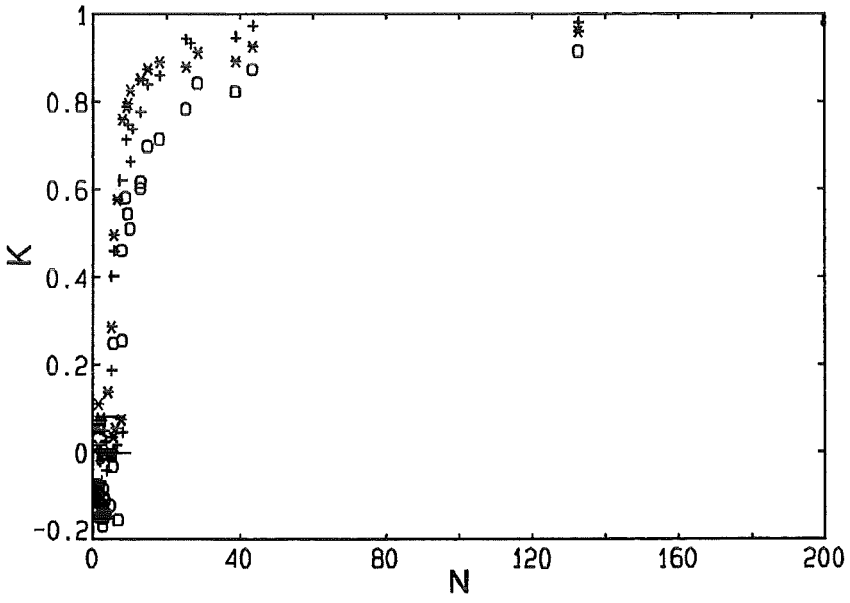

X=2.5

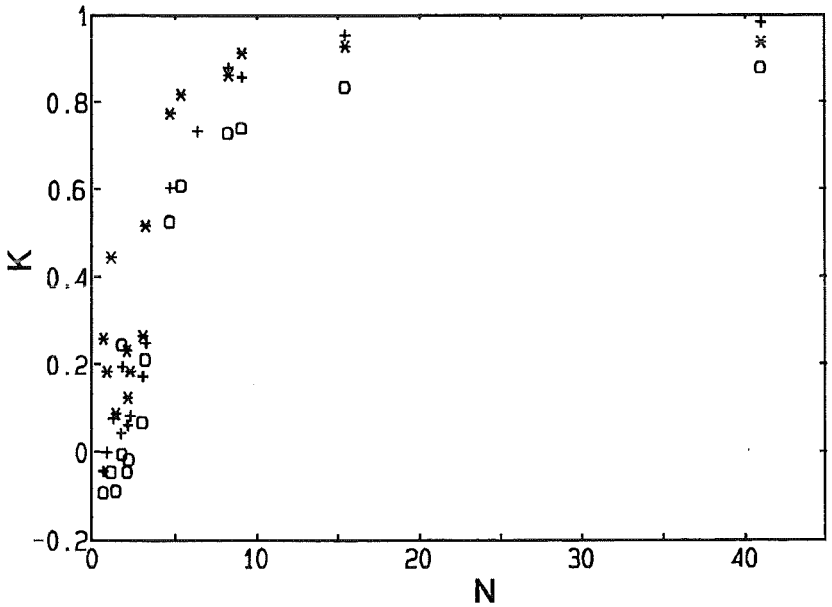

X=4.0

Fig. 4.27 Correlation coefficients for TSP signals in the downstream duct of the sharp-edged nonconducting bend ($z \approx 0.5$)

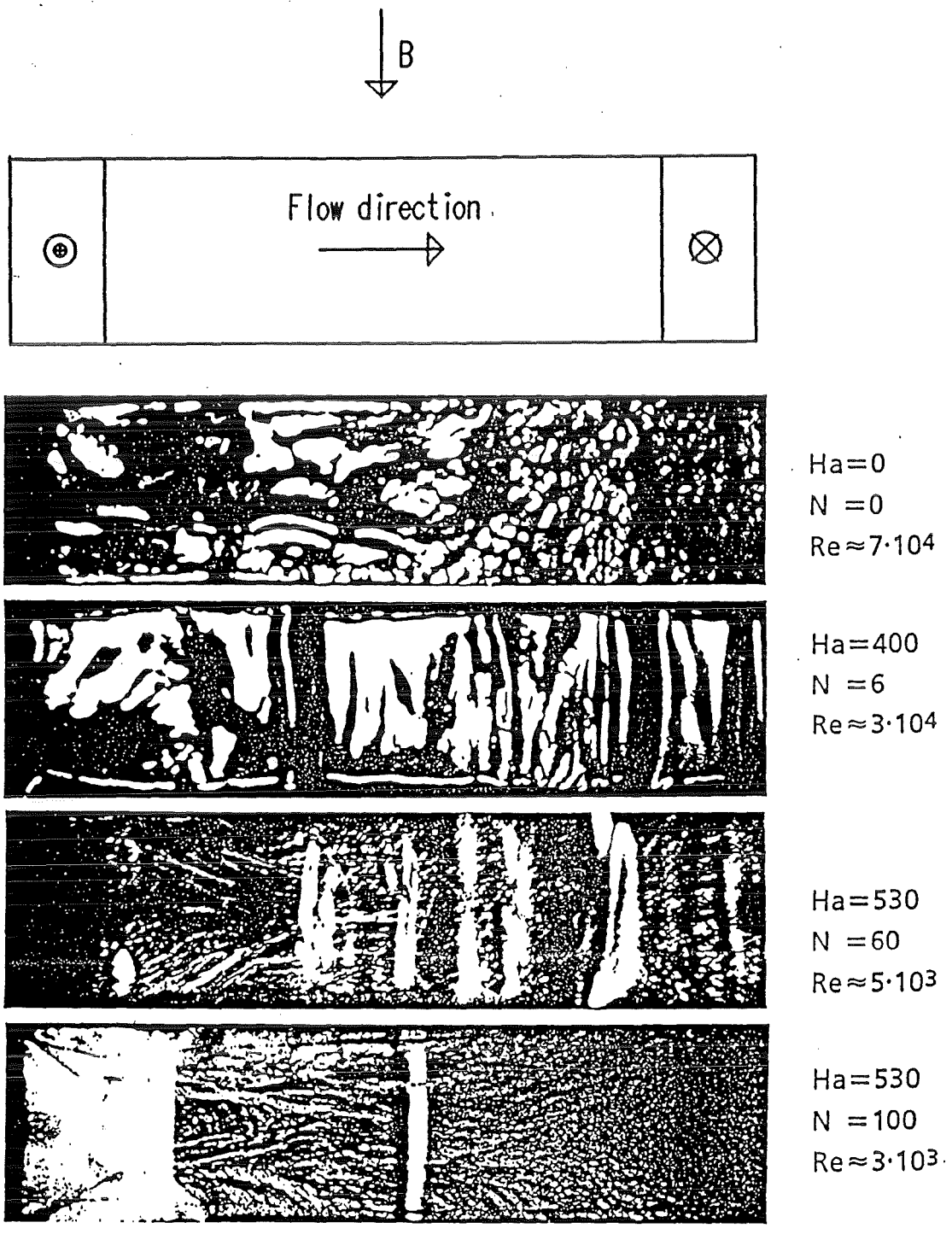

Fig. 4.28 Flow structure at mercury surface in duct downstream of nonconducting bend

positions. Figure 4.27 shows a steep increase of the coefficients at low values of N with values above 0.8 for $N > 20$.

A convincing impression of the restructuring of an ordinary turbulent flow at $N = Ha = 0$ to a 2d structure with increasing N and Ha was obtained by removing the upper wall of the test section and observing visually the liquid metal surface (Fig. 4.28). Although this changes the boundary conditions it is still believed that the main features prevail. The upper photo shows the surface for turbulent flow without magnetic field. When the magnetic field is increased, the flow structure changes impressively by becoming two-dimensional. Dips in the interface occur in the entrance region which travel downstream with a velocity comparable to the mean flow velocity. These dips are supposingly caused by the circumferential velocity component of large vortices. By decreasing the volume flow rate (increasing the Interaction parameter) the number of dips become smaller. The lowest photo corresponds to that condition where quite rarely a dip occurred.

Further details of the flow structure are revealed by analysing the time dependent signals and the energy spectra shown in the following figures for three different values of z. The abszissa of the spectra is the wave number λ which is the ratio of frequency and cross sectional mean velocity. The wave number is a crude measure for the numbers of vortices per unit length (in the present case per cm).

Figures 4.29 and 4.30 contains STP results for the nonconducting sharp-edged bend for $N \approx 140$ at different positions x. In the bend zone ($x = 0.25$) the fluctuations are largest for $z = 0.08$ which is located in the flow separation zone. With increasing z the fluctuations are somewhat smaller but still pronounced in the total cross section. With increasing x, the tendencies described already earlier are clearly seen: at the highest z value the instabilities are damped and at the lowest z the fluctuations first increase and then decrease.

Figure 4.30 contains a comparison between nonconducting and conducting bends: the larger fluctuations in the conducting bend close to the FW are clearly seen.

For heat transfer in blankets the signals close to the FW are most interesting. Figure 4.31 presents characteristic results for the conducting bend obtained with the TSP for a high value of z: The damping of the fluctuations with increasing x is very expressed.

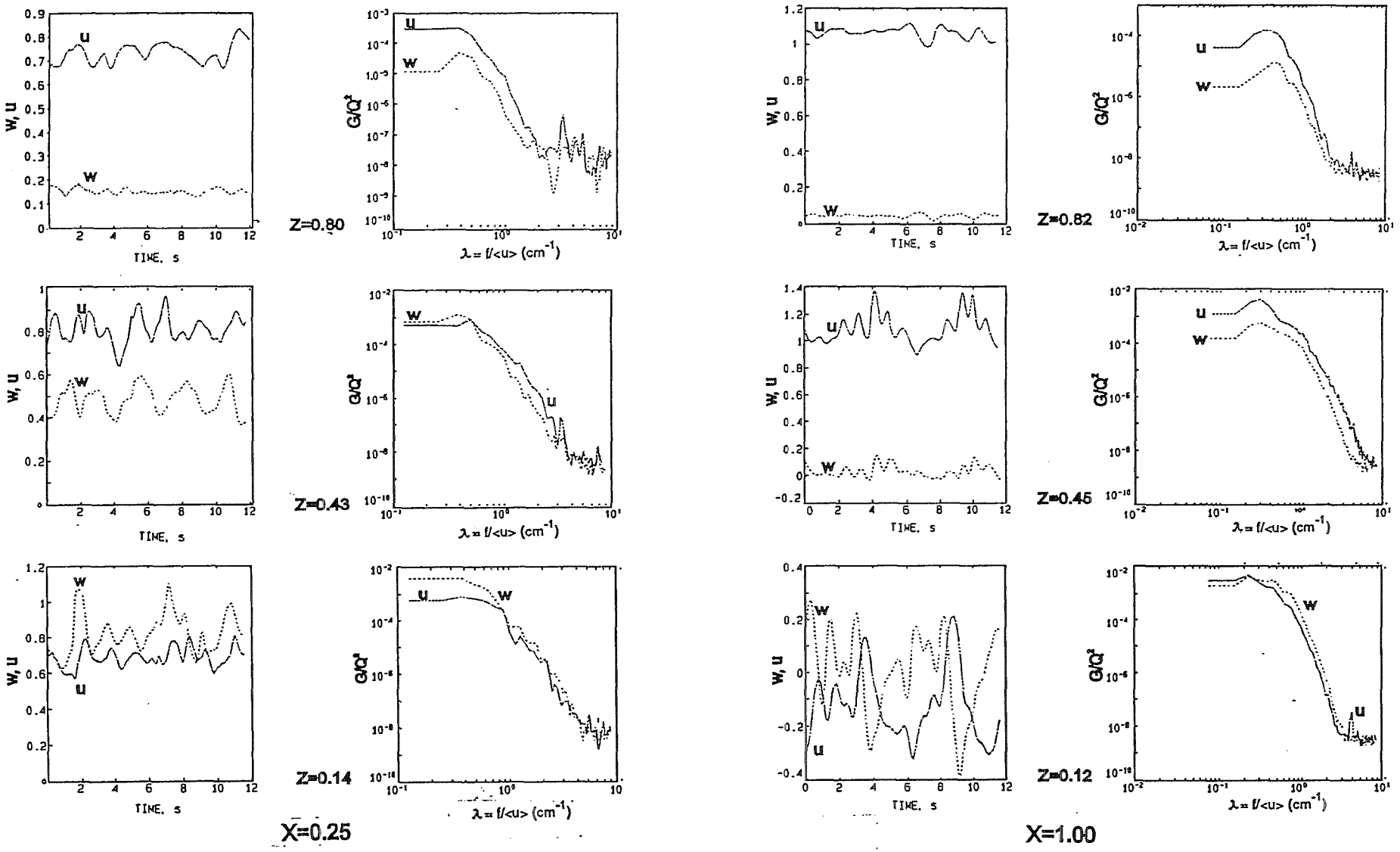

Fig. 4.29 Time dependent STP signals and spectra (nonconducting bend, N=140, Ha=530).

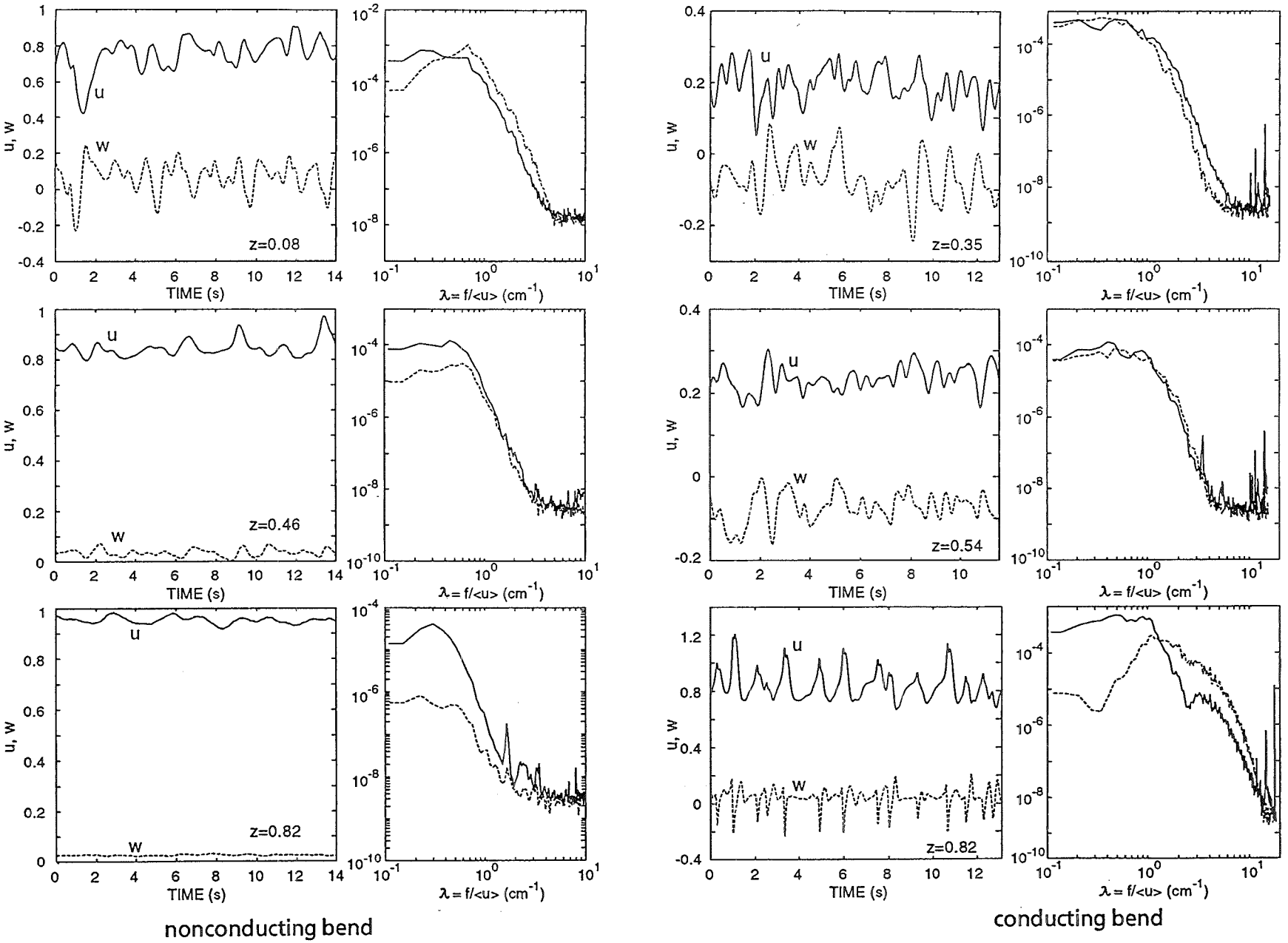

Fig. 4.30 Time dependent STP signals and spectra (C=0 and C=1.0; N≈140, Ha≈530)

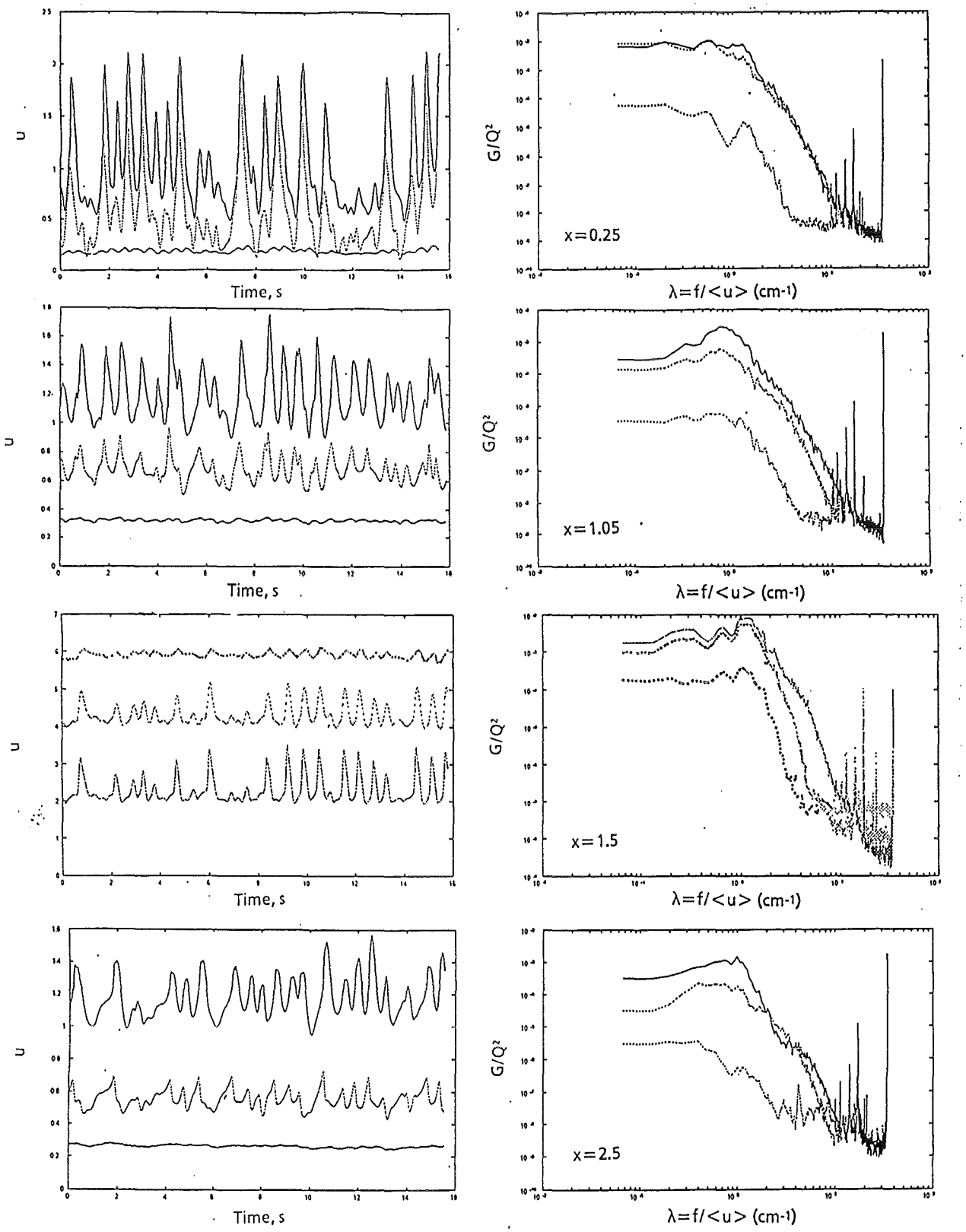

Fig. 4.31 Time dependent TSP signals and spectra (nonconducting bend, C=1.0; N≈140, Ha≈530, z≈0.85)

Figure 4.32 finally shows a comparison between STP and TSP results for N=32. A quite good agreement is observed between the signals for the u-component from the probes at y=0.

A characteristic feature of all measured spectra (only some few results were shown) is the bending of the curves at wave numbers between $0{,}5 < \lambda < 1$ and the steep drop with increasing wave number (respectively frequency). The slope of the curve in this part is typically about -5; this value is much larger than characteristic for developed MHD turbulence (compare /20 /). This slope could be explained by the fact that preferably large instabilities are generated in the bend.

4.2.4 Extrapolation for Blanket Conditions

The flow through a 90° bend perpendicular to the magnetic field seems to promote two kinds of 2d instabilities due to:

i) velocity gradients in the zone of the 90° deflection
ii) velocity gradients due to inertia effects downstream of the inner corner

The contribution i) influences mainly the turbulence promotion at the upper sidewall (the FW in a fusion reactor). The contribution ii) is first dominant at the lower sidewall but large vortices might reach the upper sidewall further downstream.

For fusion reactor blankets it is of interest if these instabilities improve the heat transfer from the FW in the bend region and how far downstream these instabilities prevail.

The occurrence of MHD turbulence in straight duct flow is often expressed in terms of

$$Re/Ha = Ha/N > (Re/Ha)_{crit},$$

where the critical value for nonconducting ducts, determined from pressure drop measurements, is of the order of 100 /5/. As mentioned earlier, the onset of turbulence promotion was observed at significantly lower values /9/. For conducting ducts it is important to know when instabilities generated in the

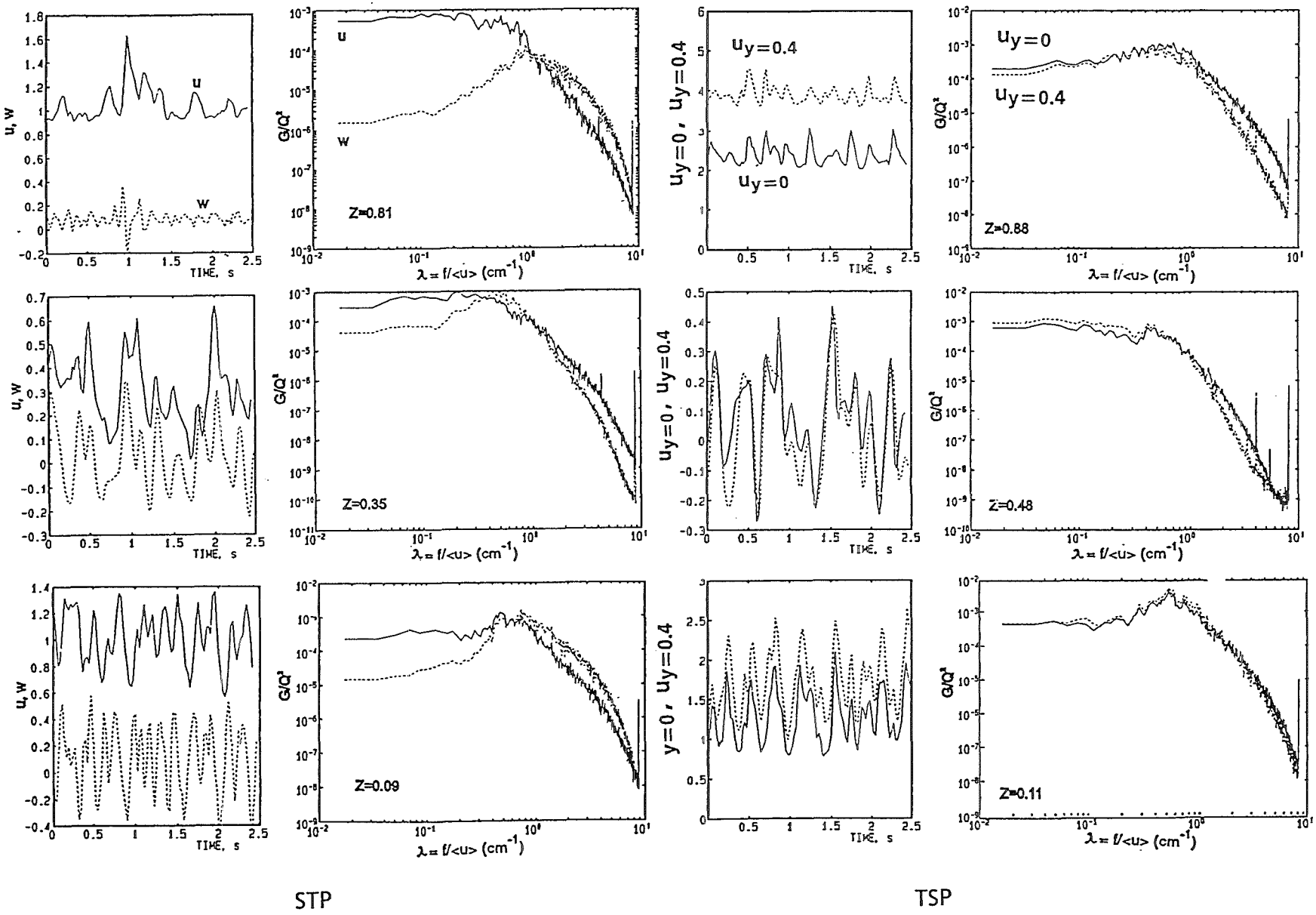

Fig. 4.32 Time dependent STP and TSP signals and spectra (nonconducting bend, N=35, Ha=530, X=2.5).

zones with strong velocity gradients due to the M-shaped velocity profile are strong enough to improve the heat transfer from the walls. These critical Re/Ha values are presently not sufficiently known for arbitrary duct flows and no work existed up to now on turbulence generation in bend flows.

For fusion reactor blankets using liquid Pb-17Li, characteristic values of the Hartmann numbers and Interaction parameters are $Ha \approx 6000$ and $N \approx 150$ corresponding to $Ha/N \approx 40$. The duct walls are either insulated ($C=0$) or thin electrically conducting ($C \approx 0.05$).

The present experiments concentrated on $Ha=530$, $N=140$ and $N=8$ which corresponds to $Re/Ha \approx 4$ and ≈ 66. Even for these low values a significant turbulence generation is observed in the bend region for both conducting and nonconducting bends. For the conducting duct this turbulence is damped out completely in the region downstream of the bend after some characteristic lengths. Here, the Hartmann braking effect in this duct with the high wall conductance ratio of $C=1$ is strong enough to prevent a permanent turbulence generation in the zones of the strong gradients of the M-shaped profile. For the nonconducting bend a damping effect in the downsteam duct is also observed. Here, the turbulence level becomes negligible when a flat velocity profile is reached.

The extrapolation of the results to blanket conditions can be performed only qualitatively: It is supposed that the bend acts as an effective turbulence promotor (or amplifier if there is already a distinct turbulence level at the bend inlet). Hot spots at the outer sidewall (the First Wall) in the bend are not expected because the turbulence level in the deflection zone is quite high.

For insulating ducts, vortices, once initiated, should exist for a nondimensional time period $\tau \sim Ha/N$, where τ is the Hartmann breaking time [22]. Therefore, for blanket-relevant conditions these vortices are expected to be damped much slower. For conducting ducts with $C >> Ha^{-0.5}$ the decay time of the vortex structure is $\tau \sim (1+C)/(CN)$, a value which also increases considerably for blanket conditions due to the much smaller value of C. Additional turbulence promotors might be required in the downstream duct in order to keep the turbulence level high.

Further investigations should be performed at more blanket-relevant parameters and attention should be paid to velocity distributions in the corner between First Wall and Hartmann wall because heat transfer is expected to be worst there.

5. SUMMARY AND CONCLUSIONS

This report summarizes the first detailed investigations on the flow structure of MHD flow in bends. These results are of interest for fusion reactor blankets where bends are connected with the First Wall which transfers the plasma heat flux to the coolant ducts. In the bend zones the formation of hot spots is of great concern.

In MHD flow the bend orientation in respect to the magnetic field direction is of significant influence on the flow structure. Two types of 90° bends were investigated: bends which were either perpendicular or partly parallel to B. The duct walls were either electrically conducting or nonconducting. The experiments were carried out in mercury flow at Hartmann numbers $0 \leq Ha \leq 550$ and Interaction parameters $0 \leq N \leq 150$. Distributions of mean velocity, velocity fluctuations and spectra were determined in different duct cross sections with traversable hot wire probes or different types of electric potential probes.

Furthermore, the velocity distributions were evaluated by theoretical analyses valid for inertialess laminarized flow.

For both types of bend orientations significant differences to the theoretical predictions occur in the bend zones due to the local influence of inertial forces. Strong flow instabilities with axis parallel to the magnetic field are observed in both cases which can persist for a quite long distance in the downstream duct, depending on the MHD parameters. Different generation mechanisms for these vortices exist: For the bend perpendicular to B, inertia effects near the inner corner play a dominant role and, for electrically conducting duct walls, the M-shaped velocity profile in the downstream duct. For bends with the downstream duct parallel to B, inertial forces in combination with the enforced M-shaping of the velocity distribution in the inlet duct are of prime importance.

In duct flows with heat transfer, such MHD flow instabilities are expected to prevent the formation of hot spots in the bend zones and might be still effective for an improved heat removal in a significant part of the downstream duct.

Further experiments are required with larger Hartmann numbers and smaller wall conductivity ratios in order to show if these instabilities exist at blanket relevant parameters.

ACKNOWLEDGEMENTS

This work was performed in the framework of the Nuclear Fusion Project of the Forschungszentrum Karlsruhe, and is supported by the European Communities within the European Fusion Technology Programme.

APPENDIX I: VELOCITY AND CORRELATION COEFFICIENT DEFINITIONS

In the report velocities are presented in dimensionless form. As normalizing factor the cross-section averaged throughout velocity Q is used (which is equal to the flow rate devided by the cross-sectional area).

The local time averaged (mean) velocity components <u>, <v>, and <w> (for flow directions, see Fig. 2.7) are given by

$$<u> = n^{-1} \sum_{i=1}^{n} u(i); \; <v> = n^{-1} \sum_{i=1}^{n} v(i); \; <w> = n^{-1},$$

where u(i), v(i) and w(i) are the instantaneous values and n is the number of discrete measurements ($n \approx 4 \cdot 10^3$ in the bpaB-exps; $n \approx 3 \cdot 10^5$ in the bpeB-exps).

The local time averaged (mean) value of the velocity fluctuation in x direction is:

$$<u'> = n^{-1} \sum_{i=1}^{n} \left((u(i) - <u>)^2 \right) 0.5$$

Corresponding definitions are used for <u'> and <w'>.

Note: The parentheses <> have been omitted in the presentations of the report !

The correlation coefficient K for the STP is defined in the following way

$$K = n^{-1} \sum_{i=1}^{n} (u(i) - <u>)(v(i) - <v>) / (<u'>) <v'>).$$

For the TSP, the correlation coefficient K'_{12} (using the probe signals at y_1 and y_2) is given by

$$K'_{12} = n^{-1} \sum_{i=1}^{n} (u(i)_1 - <u_1>)(u(i)_2 - <u_2> / (<u'_1> <u'_2>).$$

The coefficients K'_{12} and K'_{23} are defined correspondingly.

REFERENCES

/1/ S. Malang, J. Reimann, H. Sebening (Eds.), "Status report. KfK contribution to the development of DEMO-relevant test blankets for NET/ITER." Part 1 "Self-cooled liquid metal breeder blanket", Vol. 1: Summary; KfK-4907 (Karlsruhe Nuclear Research Center) (Dec. 1991).

/2/ S. Malang, M.S. Tillack (Comp.): "Development of Self-Cooled Liquid Metal Breeder Blankets", FZKA 5581, 1995.

/3/ J. Reimann, L. Barleon, I. Bucenieks, L. Bühler, L. Lenhart, S. Malang, S. Molokov, I. Platnieks, R. Stieglitz: "MHD investigations related to a self-cooled Pb-17Li blanket with poloidal-radial-toroidal ducts". Fusion Eng. & Design 27 (593-606).

/4/ L. Bühler, U. Müller: "MHD Channel flow related to self-cooled liquid-metal blanket development". KFK-Bericht 5407, 1994.

/5/ O. Lielausis, 1975: "Liquid-metal magnetohydrodynamics", Atomic Energy Review, Vol. 13, No. 3, pp. 527-581.

/6/ I.A. Platnieks, 1972: "Correlation study of turbulent velocity perturbations in a MHD-channel", Proc. Riga 7 MHD-Meeting, part 1, 31.

/7/ Y. u. B. Kolesnikov, A.B. Tsinober, 1974, "Experiment. Invest. of Two-dimens.turbulence behind a Grid", Izv. AN SSSR, Mech. Zh. i Gaza, Vol. 4, 146.

/8/ J. Sommeria, R. Moreau, 1982: "Why, how, and when, MHD turbulence becomes two-dimensional", J. Fluid Mech., Vol. 118, pp. 507-518.

/9/ S. Sukoriansky, H. Branover, E. Grenspan, 1989: "Liquid metal turbulent flow phenomena and their implications on fusion reactor blanket design", J. Lielpeteris and R. Moreau (eds), Liquid Metal Magnetohydrodynamics, by Kluwer Academic Publishers, pp. 63-69.

/10/ R. Stieglitz: "Magnetohydrodynamische Strömungen in Ein- und Mehrkanalumlenkungen". KfK 5376, Sept. 94.

/11/ R. Stieglitz, L. Barleon, L. Bühler, S. Molokov: "Magnetohydrodynamic flow in a right angle bend in a strong magnetic field", to be published in Journal of Fluid Mechanics.

/12/ S. Molokov, L. Bühler: "Liquid metal flow in a U-bend in a strong uniform magnetic field". J. Fluid Mech. (1994), pp. 325-352, Vol. 267.

/13/ J. Reimann, L. Bühler, K.-J. Mack, I. Platnieks, R. Stieglitz, F. Stumpf, 1994: "Influence of a magnetic field B on pressure drop of liquid metal flow through a T-junction perpendicular to B", 2nd Int. Conf. on Energy Transfer in Magnetohydrodynamic Flows, Aussois, France, 26-30 September.

/14/ J. Reimann, I. Bucenieks, A. Flerov, L. Heller, I. Platnieks: "MHD-Velocity Distributions in U-Bends Partly Parallel to the Magnetic Field". PAMIR - 2nd Int. Conf. on Energy Transfer in Magnetohydrodynamic Flows. Sept. 26-30, 1994, Aussois, France.

/15/ J. Reimann, I. Bucenieks, L. Bühler, S. Dementjev, A. Florev, I. Platnieks: "Flow structure downstream of a 90° bend perpendicular to the magnetic field". MAHYD '95, Riga, August 1995.

/16/ A. Kyrlidis, R.A. Brown, S.S. Walker, "Creeping flow of a conducting fluid past axisymmetric bodies in the presence of an aligned magnetic field", Phys. Fluids A2(12), pp. 2230-2239, Dec. 1990

/17/ M. Lake, "Velocity measurements in regions of upstream influence of a body in aligned-fields MHD flow", J. Fluid Mech, 1971, Vol. 50, part 2, pp. 209-231

/18/ P.S. Lykoudis, P.F. Dunn, 1973, "Magneto fluid mechanic heat transfer from hot film probes", Int. J. Heat and Mass Transfer, Vol. 16, pp. 1439-1452.

/19/ L. Bühler, 1995, "Magnetohydrodynamic flows in ducts of arbitrary geometries in strong nonuniform magnetic fields". Fusion Technology Vol. 27, pp. 3-24.

/20/ H. Branover, 1978, "Magnetohydrodynamic Flow in Ducts", John Wiley & Sons, New York/Toronto/Jerusalem.

/21/ H. Schade, E. Kunz, 1989, "Strömungslehre", Walter de Gruyter, Berlin/New York.

/22/ R. Moreau, 1990, "Magnetohydrodynamics", Kluwer Academic Publishers, Dortrecht/Boston/London.